

PDF hosted at the Radboud Repository of the Radboud University Nijmegen

The following full text is a preprint version which may differ from the publisher's version.

For additional information about this publication click this link.

<http://hdl.handle.net/2066/124908>

Please be advised that this information was generated on 2020-09-19 and may be subject to change.

Measurement of the Branching Fractions and Forward-Backward Asymmetries of the Z^0 into Light Quarks

The OPAL Collaboration

Abstract

Using approximately 4.3 million hadronic Z^0 decays collected with the OPAL detector at LEP between 1990 and 1995, we measure the branching fractions of the Z^0 into up-type and down-type light quarks, R_q , and the forward-backward asymmetries, $A_{FB}(q)$, using high-momentum stable particles as a tag. Adopting a method that employs double tagged events to determine the flavour tagging efficiencies, and assuming the flavour independence of strong interactions and SU(2) isospin symmetry, we measure:

$$\begin{aligned} \frac{R_{d,s}}{(R_d + R_u + R_s)} &= 0.371 \pm 0.016 \text{ (stat.)} \pm 0.016 \text{ (syst.)} \text{ and} \\ A_{FB}(d,s) &= 0.068 \pm 0.035 \text{ (stat.)} \pm 0.011 \text{ (syst.)} , \end{aligned}$$

assuming the branching fractions and forward-backward asymmetries of down and strange quarks to be equal. The results are essentially free of assumptions based on hadronisation models. These results are in agreement with the Standard Model expectations and are used to infer the left and right handed couplings of strange/down quarks to the Z^0 , yielding

$$g_L^{d,s} = -0.44_{-0.09}^{+0.13} \quad \text{and} \quad g_R^{d,s} = +0.13_{-0.17}^{+0.15} .$$

The results for the up quark, $R_u/(R_d + R_u + R_s) = 0.258 \pm 0.031 \text{ (stat.)} \pm 0.032 \text{ (syst.)}$ and $A_{FB}(u) = 0.040 \pm 0.067 \text{ (stat.)} \pm 0.028 \text{ (syst.)}$, are fully negatively correlated and almost completely positively correlated, respectively, with the corresponding down-type results.

(Submitted to Zeitschrift für Physik C)

The OPAL Collaboration

K. Ackerstaff⁸, G. Alexander²³, J. Allison¹⁶, N. Altekamp⁵, K.J. Anderson⁹, S. Anderson¹²,
S. Arcelli², S. Asai²⁴, D. Axen²⁹, G. Azuelos^{18,a}, A.H. Ball¹⁷, E. Barberio⁸, R.J. Barlow¹⁶,
R. Bartoldus³, J.R. Batley⁵, S. Baumann³, J. Bechtluft¹⁴, C. Beeston¹⁶, T. Behnke⁸, A.N. Bell¹,
K.W. Bell²⁰, G. Bella²³, S. Bentvelsen⁸, P. Berlich¹⁰, S. Bethke¹⁴, O. Biebel¹⁴, A. Biguzzi⁵,
S.D. Bird¹⁶, V. Blobel²⁷, I.J. Bloodworth¹, J.E. Bloomer¹, M. Bobinski¹⁰, P. Bock¹¹,
D. Bonacorsi², M. Boutemeur³⁴, B.T. Bouwens¹², S. Braibant¹², L. Brigliadori², R.M. Brown²⁰,
H.J. Burckhart⁸, C. Burgard⁸, R. Bürgin¹⁰, P. Capiluppi², R.K. Carnegie⁶, A.A. Carter¹³,
J.R. Carter⁵, C.Y. Chang¹⁷, D.G. Charlton^{1,b}, D. Chrisman⁴, P.E.L. Clarke¹⁵, I. Cohen²³,
J.E. Conboy¹⁵, O.C. Cooke¹⁶, M. Cuffiani², S. Dado²², C. Dallapiccola¹⁷, G.M. Dallavalle², S. De
Jong¹², L.A. del Pozo⁴, K. Desch³, M.S. Dixit⁷, E. do Couto e Silva¹², M. Doucet¹⁸,
E. Duchovni²⁶, G. Duckeck³⁴, I.P. Duerdoth¹⁶, D. Eatough¹⁶, J.E.G. Edwards¹⁶,
P.G. Estabrooks⁶, H.G. Evans⁹, M. Evans¹³, F. Fabbri², M. Fanti², A.A. Faust³⁰, F. Fiedler²⁷,
M. Fierro², H.M. Fischer³, I. Fleck⁸, R. Folman²⁶, D.G. Fong¹⁷, M. Foucher¹⁷, A. Fürties⁸,
D.I. Futyan¹⁶, P. Gagnon⁷, J.W. Gary⁴, J. Gascon¹⁸, S.M. Gascon-Shotkin¹⁷, N.I. Geddes²⁰,
C. Geich-Gimbel³, T. Geralis²⁰, G. Giacomelli², P. Giacomelli⁴, R. Giacomelli², V. Gibson⁵,
W.R. Gibson¹³, D.M. Gingrich^{30,a}, D. Glenzinski⁹, J. Goldberg²², M.J. Goodrick⁵, W. Gorn⁴,
C. Grandi², E. Gross²⁶, J. Grunhaus²³, M. Gruwe⁸, C. Hajdu³², G.G. Hanson¹², M. Hansroul⁸,
M. Hapke¹³, C.K. Hargrove⁷, P.A. Hart⁹, C. Hartmann³, M. Hauschild⁸, C.M. Hawkes⁵,
R. Hawkings²⁷, R.J. Hemingway⁶, M. Herndon¹⁷, G. Herten¹⁰, R.D. Heuer⁸, M.D. Hildreth⁸,
J.C. Hill⁵, S.J. Hillier¹, T. Hilse¹⁰, P.R. Hobson²⁵, R.J. Homer¹, A.K. Honma^{28,a}, D. Horváth^{32,c},
R. Howard²⁹, D.E. Hutchcroft⁵, P. Igo-Kemenes¹¹, D.C. Imrie²⁵, M.R. Ingram¹⁶, K. Ishii²⁴,
A. Jawahery¹⁷, P.W. Jeffreys²⁰, H. Jeremie¹⁸, M. Jimack¹, A. Joly¹⁸, C.R. Jones⁵, G. Jones¹⁶,
M. Jones⁶, U. Jost¹¹, P. Jovanovic¹, T.R. Junk⁸, D. Karlen⁶, V. Kartvelishvili¹⁶, K. Kawagoe²⁴,
T. Kawamoto²⁴, R.K. Keeler²⁸, R.G. Kellogg¹⁷, B.W. Kennedy²⁰, J. Kirk²⁹, A. Klier²⁶,
S. Kluth⁸, T. Kobayashi²⁴, M. Kobel¹⁰, D.S. Koetke⁶, T.P. Kokott³, M. Kolrep¹⁰,
S. Komamiya²⁴, T. Kress¹¹, P. Krieger⁶, J. von Krogh¹¹, P. Kyberd¹³, G.D. Lafferty¹⁶,
R. Lahmann¹⁷, W.P. Lai¹⁹, D. Lanske¹⁴, J. Lauber¹⁵, S.R. Lautenschlager³¹, J.G. Layter⁴,
D. Lazic²², A.M. Lee³¹, E. Lefebvre¹⁸, D. Lellouch²⁶, J. Letts¹², L. Levinson²⁶, S.L. Lloyd¹³,
F.K. Loebinger¹⁶, G.D. Long²⁸, M.J. Losty⁷, J. Ludwig¹⁰, A. Macchiolo², A. Macpherson³⁰,
M. Mannelli⁸, S. Marcellini², C. Markus³, A.J. Martin¹³, J.P. Martin¹⁸, G. Martinez¹⁷,
T. Mashimo²⁴, P. Mättig³, W.J. McDonald³⁰, J. McKenna²⁹, E.A. Mckigney¹⁵, T.J. McMahon¹,
R.A. McPherson⁸, F. Meijers⁸, S. Menke³, F.S. Merritt⁹, H. Mes⁷, J. Meyer²⁷, A. Micheli²,
G. Mikenberg²⁶, D.J. Miller¹⁵, A. Mincer^{22,e}, R. Mir²⁶, W. Mohr¹⁰, A. Montanari², T. Mori²⁴,
M. Morii²⁴, U. Müller³, K. Nagai²⁶, I. Nakamura²⁴, H.A. Neal⁸, B. Nellen³, R. Nisius⁸,
S.W. O’Neale¹, F.G. Oakham⁷, F. Odorici², H.O. Ogren¹², N.J. Oldershaw¹⁶, M.J. Oreglia⁹,
S. Orito²⁴, J. Pálincás^{33,d}, G. Pásztor³², J.R. Pater¹⁶, G.N. Patrick²⁰, J. Patt¹⁰, M.J. Pearce¹,
S. Petzold²⁷, P. Pfeifenschneider¹⁴, J.E. Pilcher⁹, J. Pinfold³⁰, D.E. Plane⁸, P. Poffenberger²⁸,
B. Poli², A. Posthaus³, H. Przysiezniak³⁰, D.L. Rees¹, D. Rigby¹, S. Robertson²⁸, S.A. Robins²²,
N. Rodning³⁰, J.M. Roney²⁸, A. Rooke¹⁵, E. Ros⁸, A.M. Rossi², M. Rosvick²⁸, P. Routenburg³⁰,
Y. Rozen²², K. Runge¹⁰, O. Runolfsson⁸, U. Ruppel¹⁴, D.R. Rust¹², R. Rylko²⁵, K. Sachs¹⁰,
T. Saeki²⁴, E.K.G. Sarkisyan²³, C. Sbarra²⁹, A.D. Schaile³⁴, O. Schaile³⁴, F. Scharf³,
P. Scharff-Hansen⁸, P. Schenk³⁴, J. Schieck¹¹, P. Schleper¹¹, B. Schmitt⁸, S. Schmitt¹¹,
A. Schöning⁸, M. Schröder⁸, H.C. Schultz-Coulon¹⁰, M. Schulz⁸, M. Schumacher³, C. Schwick⁸,
W.G. Scott²⁰, T.G. Shears¹⁶, B.C. Shen⁴, C.H. Shepherd-Themistocleous⁸, P. Sherwood¹⁵,
G.P. Siroli², A. Sittler²⁷, A. Skillman¹⁵, A. Skuja¹⁷, A.M. Smith⁸, G.A. Snow¹⁷, R. Sobie²⁸,

S. Söldner-Rembold¹⁰, R.W. Springer³⁰, M. Sproston²⁰, K. Stephens¹⁶, J. Steuerer²⁷,
B. Stockhausen³, K. Stoll¹⁰, D. Strom¹⁹, P. Szymanski²⁰, R. Tafirout¹⁸, S.D. Talbot¹,
S. Tanaka²⁴, P. Taras¹⁸, S. Tarem²², R. Teuscher⁸, M. Thiergen¹⁰, M.A. Thomson⁸, E. von
Törne³, S. Towers⁶, I. Trigger¹⁸, E. Tsur²³, A.S. Turcot⁹, M.F. Turner-Watson⁸, P. Utzat¹¹,
R. Van Kooten¹², M. Verzocchi¹⁰, P. Vikas¹⁸, E.H. Vokurka¹⁶, H. Voss³, F. Wäckerle¹⁰,
A. Wagner²⁷, C.P. Ward⁵, D.R. Ward⁵, P.M. Watkins¹, A.T. Watson¹, N.K. Watson¹,
P.S. Wells⁸, N. Wermes³, J.S. White²⁸, B. Wilkens¹⁰, G.W. Wilson²⁷, J.A. Wilson¹, G. Wolf²⁶,
T.R. Wyatt¹⁶, S. Yamashita²⁴, G. Yekutieli²⁶, V. Zacek¹⁸, D. Zer-Zion⁸

¹School of Physics and Space Research, University of Birmingham, Birmingham B15 2TT, UK

²Dipartimento di Fisica dell' Università di Bologna and INFN, I-40126 Bologna, Italy

³Physikalisches Institut, Universität Bonn, D-53115 Bonn, Germany

⁴Department of Physics, University of California, Riverside CA 92521, USA

⁵Cavendish Laboratory, Cambridge CB3 0HE, UK

⁶Ottawa-Carleton Institute for Physics, Department of Physics, Carleton University, Ottawa, Ontario K1S 5B6, Canada

⁷Centre for Research in Particle Physics, Carleton University, Ottawa, Ontario K1S 5B6, Canada

⁸CERN, European Organisation for Particle Physics, CH-1211 Geneva 23, Switzerland

⁹Enrico Fermi Institute and Department of Physics, University of Chicago, Chicago IL 60637, USA

¹⁰Fakultät für Physik, Albert Ludwigs Universität, D-79104 Freiburg, Germany

¹¹Physikalisches Institut, Universität Heidelberg, D-69120 Heidelberg, Germany

¹²Indiana University, Department of Physics, Swain Hall West 117, Bloomington IN 47405, USA

¹³Queen Mary and Westfield College, University of London, London E1 4NS, UK

¹⁴Technische Hochschule Aachen, III Physikalisches Institut, Sommerfeldstrasse 26-28, D-52056 Aachen, Germany

¹⁵University College London, London WC1E 6BT, UK

¹⁶Department of Physics, Schuster Laboratory, The University, Manchester M13 9PL, UK

¹⁷Department of Physics, University of Maryland, College Park, MD 20742, USA

¹⁸Laboratoire de Physique Nucléaire, Université de Montréal, Montréal, Quebec H3C 3J7, Canada

¹⁹University of Oregon, Department of Physics, Eugene OR 97403, USA

²⁰Rutherford Appleton Laboratory, Chilton, Didcot, Oxfordshire OX11 0QX, UK

²²Department of Physics, Technion-Israel Institute of Technology, Haifa 32000, Israel

²³Department of Physics and Astronomy, Tel Aviv University, Tel Aviv 69978, Israel

²⁴International Centre for Elementary Particle Physics and Department of Physics, University of Tokyo, Tokyo 113, and Kobe University, Kobe 657, Japan

²⁵Brunel University, Uxbridge, Middlesex UB8 3PH, UK

²⁶Particle Physics Department, Weizmann Institute of Science, Rehovot 76100, Israel

²⁷Universität Hamburg/DESY, II Institut für Experimental Physik, Notkestrasse 85, D-22607 Hamburg, Germany

²⁸University of Victoria, Department of Physics, P O Box 3055, Victoria BC V8W 3P6, Canada

²⁹University of British Columbia, Department of Physics, Vancouver BC V6T 1Z1, Canada

³⁰University of Alberta, Department of Physics, Edmonton AB T6G 2J1, Canada

³¹Duke University, Dept of Physics, Durham, NC 27708-0305, USA

³²Research Institute for Particle and Nuclear Physics, H-1525 Budapest, P O Box 49, Hungary

³³Institute of Nuclear Research, H-4001 Debrecen, P O Box 51, Hungary

³⁴Ludwigs-Maximilians-Universität München, Sektion Physik, Am Coulombwall 1, D-85748 Garching, Germany

^a and at TRIUMF, Vancouver, Canada V6T 2A3

^b and Royal Society University Research Fellow

^c and Institute of Nuclear Research, Debrecen, Hungary

^d and Department of Experimental Physics, Lajos Kossuth University, Debrecen, Hungary

^e and Depart of Physics, New York University, NY 1003, USA

1 Introduction

One of the basic assumptions of the Standard Model [1] is flavour universality, namely that apart from mass effects, the gauge couplings of all fermions depend only on their charge, weak isospin, and colour. While this assumption has been experimentally tested to high accuracy in the charged lepton sector, results on quarks are generally less precise. The large number of Z^0 decays recorded at the LEP e^+e^- collider opens the possibility for high-precision measurements of the Z^0 couplings to several individual fermion species. Accurate measurements exist particularly for the bottom quarks, and to a lesser extent for the charm quark [2]. However, at LEP, few measurements exist of the couplings of individual up, down, and strange quarks to the neutral weak current. The couplings of up and down quarks have been obtained at low Q^2 from lepton-nucleon scattering and from atomic parity violation and are in agreement with the Standard Model expectations [3]. Direct measurements of light flavours on the Z^0 resonance are scarce. Apart from the overall hadronic width, the yield of photon radiation from quarks is particularly sensitive to up-type quarks [4]. A first measurement of the strange quark forward-backward asymmetry, which is dependent on hadronisation models, has been published in [5].

In this paper we determine the decay branching fractions of the Z^0 into up-type and down-type light quarks and the forward-backward asymmetries with only few model assumptions, as introduced in [6]. The method relies on the property that a high-energy particle in a jet has a flavour correlation with the primary quark. Since charm and bottom quarks do not contribute much to the production of long-lived hadrons with a significant fraction of the beam energy, a selection of events with π^\pm , K^\pm , $p(\bar{p})$, K_S^0 , or $\Lambda(\bar{\Lambda})$ baryons of high energy provides rather pure samples of light flavours¹. The main challenge is to determine the relative yields of up, down, and strange quarks in such event samples. This is achieved by using the information from double tagged events, where two high-momentum particles are found in opposite event hemispheres, together with some general hadronisation symmetries.

The method of measuring the branching fractions and the forward-backward asymmetries is described in detail in Section 2. The elements of the OPAL detector pertinent to this analysis and the basic event selection are presented in Sections 3 and 4. In Section 5 we describe the estimation of the charm and bottom backgrounds in our high-momentum samples and in Section 6 the electroweak observables are determined for up-type and down-type light quarks. Systematic uncertainties are evaluated in Section 7 and the conclusions are given in Section 8.

2 The Method

The observed long range charge correlations in e^+e^- events [7] show that the particle with the highest energy in a jet tends to carry the quantum numbers of the primary quark. Thus, jets from primary strange quarks lead to high-energy strange hadrons, for example, and primary up and down quarks lead to high-energy pions and protons. We base our analysis on this property and tag light quark events by identifying high-energy charged pions, charged and neutral kaons, protons, and Λ baryons with $x_p = 2p_h/E_{\text{cm}} \geq 0.5$, where p_h is the momentum of the tagging

¹Unless explicitly stated otherwise, charge conjugation of the tagging particle and primary quark types is implied throughout this paper.

hadron, h , and E_{cm} is the centre-of-mass energy of the event. The value of $x_p > 0.5$ is chosen to minimise the statistical and systematic uncertainties. We now make a general discussion of the method without considering the detector.

2.1 Method to Determine the Branching Fractions

If the relations between particle types and primary flavours were unambiguous, double tagged events, in which a tagging hadron is found in each of the event hemispheres, could be used to determine the flavour tagging efficiencies in a straightforward way. The method would then be essentially free from uncertainties due to the detailed properties of the flavour tag and detector effects. Almost no ambiguity exists for bottom particles, where the double tagging method has been successfully applied (see [8], for example). On the other hand, high-energy light-flavour mesons and baryons can be produced by processes other than the hadronisation of primary quarks. Leading mesons contain a quark and an antiquark, either of which could be the quark into which the Z^0 decayed directly, which introduces some ambiguity. In addition, decays of these so-called primary hadrons and of particles produced from the hadronisation sea tend to obscure further the primary flavour source of each particle type. Thus, each particle species is produced from a mixture of several primary quark flavours. Neglecting correlations, the number of tagged event hemispheres (as defined by the thrust axis) and the number of double tagged events can be expressed as:

$$\frac{N_h}{N_{\text{had}}} = 2 \sum_{q=d,u,s,c,b} \eta_q^h R_q \quad \text{and} \quad (1)$$

$$\frac{N_{hh'}}{N_{\text{had}}} = \sum_{q=d,u,s,c,b} \eta_q^h \eta_q^{h'} R_q, \quad (2)$$

where N_h is the number of hemispheres with a tagging hadron $h = \pi^\pm, K^\pm, p(\bar{p}), K_S^0, \Lambda(\bar{\Lambda})$, N_{had} is the number of hadronic Z^0 decays, and $N_{hh'}$ is the number of double tagged events with tagging particle types h and h' . The η_q^h denote the fraction of hemispheres with a primary quark flavour q which are tagged by a hadron of type h , and R_q is the hadronic branching fraction of the Z^0 to quarks q :

$$R_q = \frac{\Gamma_{Z^0 \rightarrow q\bar{q}}}{\Gamma_{\text{had}}}. \quad (3)$$

As will be shown in Section 5, the charm and bottom fractions can be determined separately in a straightforward way, leaving fifteen unknown η_q^h and three unknown R_q . On the other hand, for the five tagging particle types we consider, there is a system of five equations for tagged hemispheres (Eq. 1) and fifteen equations for double tagged event types (Eq. 2). Due to the non-linearity and degeneracy of the equation system, it is not solvable and additional constraints have to be found to obtain a solution.

As discussed in detail in [6], the necessary constraints can be derived from SU(2) isospin symmetry and the flavour independence of QCD. We use the following hadronisation relations:

$$\eta_d^{\pi^\pm} = \eta_u^{\pi^\pm}, \quad (4)$$

$$\eta_d^{K^0(\bar{K}^0)} = \eta_u^{K^\pm}, \quad (5)$$

$$\eta_u^{K^0(\bar{K}^0)} = \eta_d^{K^\pm}, \quad (6)$$

$$\eta_s^{K^0(\bar{K}^0)} = \eta_s^{K^\pm}, \text{ and} \quad (7)$$

$$\eta_u^{\Lambda(\bar{\Lambda})} = \eta_d^{\Lambda(\bar{\Lambda})}. \quad (8)$$

Note that $K^0(\bar{K}^0)$ implies K_S^0 plus K_L^0 . Small deviations from these relations are discussed later in Section 7. In addition, the overall normalisation $\sum R_q = 1$ provides another constraint:

$$R_u + R_d + R_s = 1 - R_c - R_b = 0.620 \pm 0.010, \quad (9)$$

where the LEP measurements [2] of R_b and R_c can be used to constrain the sum of the light-flavour branching fractions. To be independent of the measurements of the heavy flavour fractions, we also express our results in terms of:

$$R'_q = \frac{\Gamma_{q\bar{q}}}{\Gamma_{d\bar{d}} + \Gamma_{u\bar{u}} + \Gamma_{s\bar{s}}} = \frac{R_q}{R_d + R_u + R_s} \quad (10)$$

The R'_q are related to the R_q via $R_q = R'_q(1 - R_b - R_c)$.

These constraints are still not sufficient to allow the system to be solved. Motivated by the weak isospin structure of the Standard Model, we assume $R_d = R_s$, thereby reducing the number of unknown R_q and making possible a solution of the equation system.

2.2 Method to Determine the Forward-Backward Asymmetries

The other directly measurable electroweak-related observable is the forward-backward asymmetry A_{FB}^h of a hadron h :

$$A_{FB}^h = \frac{N_h(\cos\theta > 0) - N_h(\cos\theta < 0)}{N_h}, \quad (11)$$

where θ is the angle of the tagging hadron h with respect to the incoming electron direction. The relation between this directly observable asymmetry and the desired forward-backward asymmetries of the quarks is given by [6]:

$$A_{FB}^h = \sum_q \left\{ s_q f_q^h (2r_q^h - 1) \right\} A_{FB}(q), \quad (12)$$

where the reliabilities of the charge tag are given by $r_q^h = N_{h,q}^{\text{correct}}/N_{h,q}$, $N_{h,q}^{\text{correct}}$ being the number of hadrons h which have the same sign of the charge as the primary quark q . The reliability therefore takes into account dilutions due to the misidentification of the sign of the charges of the quarks, s_q . Finally, f_q^h is the fraction of tagged hadrons h stemming from a primary quark q , i.e. $f_q^h = (\eta_q^h R_q)/(\sum_{q'} \eta_{q'}^h R_{q'})$. Therefore, the forward-backward asymmetries $A_{FB}(q)$ can be determined only after the η_q^h , R_q , and reliabilities r_q^h are known. The reliabilities can be determined from the ratio of double tagged events with tagging particles of opposite charge, $N_{hh'}^{\text{OPP}}$ over the total number of double tagged events, $N_{hh'}$:

$$\frac{N_{hh'}^{\text{OPP}}}{N_{hh'}} = \sum_q \frac{\eta_q^h \eta_q^{h'} R_q}{(\sum_{q'} \eta_{q'}^h \eta_{q'}^{h'} R_{q'})} \left\{ r_q^h r_q^{h'} + (1 - r_q^h)(1 - r_q^{h'}) \right\}. \quad (13)$$

Since the K_S^0 provides no information on the charge of the primary quark, we restrict the determination of the forward-backward asymmetries to charged pions, charged kaons, protons, and Λ baryons. With these four hadron types we obtain four measurements of A_{FB}^h and ten ratios $N_{hh'}^{\text{OPP}}/N_{hh'}$ which must be used to determine 12 unknown light flavour reliabilities and the three asymmetries $A_{FB}(q)$. Here we assume that the heavy flavour terms can be determined separately, as will be shown later in Section 5. As for the solution of the equation system for the branching fractions, we invoke hadronisation symmetries based on SU(2) isospin invariance to reduce the number of unknown reliabilities:

$$r_d^{\pi^\pm} = r_u^{\pi^\pm} , \quad (14)$$

$$r_s^{\pi^\pm} = 0.5 , \text{ and} \quad (15)$$

$$r_d^{\Lambda(\bar{\Lambda})} = 1 - r_u^{\Lambda(\bar{\Lambda})} . \quad (16)$$

Note that for the baryons (the proton and Λ), the tagging hadron carries the sign of the baryon number of the primary quark, not the electric charge, so that $r_q^{\text{baryon}} < 0.5$ for down-type quarks and $r_q^{\text{baryon}} > 0.5$ for up-type quarks. In addition, in order to solve the equation system we must assume that (see [6]):

$$r_d^{\text{K}^\pm} = 0.20 \pm 0.10 , \quad (17)$$

where the value is taken from the JETSET model [9] and is assigned a large error to take into account uncertainties in the JETSET modelling. This particular reliability is chosen as the one to be fixed since $f_d^{\text{K}^\pm}$ is small compared to the other flavour fractions. Therefore, even a large uncertainty in $r_d^{\text{K}^\pm}$ does not affect significantly the final result.

In the preceding discussion we have ignored biases due to geometrical and kinematic constraints which have to be taken into account. Requiring a high-energy hadron in an event reduces the phase space for gluon bremsstrahlung and thus introduces a kinematic correlation between the event hemispheres. Similarly, restrictions on the geometrical acceptance introduce corrections to the equation systems we use. We parametrise this correction by a factor ρ , so that the double tagging probability, $\eta_q^{hh'}$, is given by:

$$\eta_q^{hh'} = \rho \eta_q^h \eta_q^{h'} . \quad (18)$$

In the ideal case of no bias, $\rho = 1$. Model calculations suggest [6] that this correlation is independent of the tagging particle type and the primary quark flavour and is approximately 1.07 for a sample of tagging hadrons with $x_p > 0.5$ without experimental cuts and neglecting detector effects, and is essentially due to gluon bremsstrahlung. In order for the measurement of the light-flavour electroweak parameters to be as model independent as possible, we let ρ be a free parameter in the equation system but assume that it is independent of the tagging hadron species. Note that ρ is largely uncorrelated with the other parameters.

3 The OPAL Detector

The OPAL detector is described in detail in [10]. Here we summarise only the features of the detector which are important for this analysis.

Central to this study is the determination of the momentum and the identity of different types of charged hadrons and neutral hadrons which decay to stable charged particles. OPAL has a system of tracking devices inside a solenoid which provides a magnetic field of 0.435 T. A charged track momentum resolution of $\sigma_p/p = 0.02 \oplus 0.0015 p_t$, where p_t is the component of the total track momentum p in the plane perpendicular to the beam axis measured in GeV, has been achieved. The innermost part is a silicon microvertex detector [11], surrounded by three drift chambers: a vertex detector, a large volume jet chamber which provides up to 159 space points per track, and z -chambers to give a more precise measurement of the polar angle of charged tracks². The large number of measurements in the jet chamber also provides a determination of the specific ionisation energy loss, dE/dx , with a resolution of $\sigma(dE/dx)/(dE/dx) \sim 0.035$ [12] for well-separated tracks with $|\cos\theta| < 0.7$. This resolution allows the identification of charged pions, charged kaons, and protons up to the highest particle momenta [13]. The large radius of the jet chamber ($R = 185$ cm) also allows a high reconstruction efficiency for large-momentum, weakly decaying hadrons with relatively long decay lengths, such as $K_S^0 \rightarrow \pi^+\pi^-$ and $\Lambda \rightarrow p\pi^-$.

To estimate the contributions from bottom quarks, we also identify secondary vertices from b hadron decays [14] and use electron and muon identification [15, 16] to tag semi-leptonic bottom decays. The identification of a secondary vertex profits particularly from the high-precision measurements in the silicon microvertex detector. The lepton identification is largely based on the electromagnetic calorimeter, which consists of 11 704 lead glass blocks which subtend a solid angle of 40×40 mrad, and muon chambers which are placed behind an average of eight absorption lengths of detector material.

To determine detector efficiencies and possible detector biases, we use a sample of approximately eight million simulated hadronic Z^0 decays generated with the JETSET model [9] and passed through a detailed simulation of the OPAL detector [17]. The fragmentation parameters have been tuned to describe overall event shapes and distributions as described in detail in [18]. Events are generated with two versions of JETSET. Events with JETSET 7.3 use a simulation of the detector up to and including 1993, while the JETSET 7.4 events use a simulation of the detector corresponding to subsequent years.

4 Event Selection

The analysis is based on approximately 4.3 million multihadronic Z^0 decays collected between 1990 and 1995. Of these events approximately 90% were collected at centre-of-mass energies within ± 200 MeV of the Z^0 mass, and the rest of the events within ± 3 GeV above and below the Z^0 peak. The standard OPAL requirements for the multihadronic event selection are given in [19]. To enrich the light-flavour fraction we retain only those events which have at least one well measured charged track, a K_S^0 , or a Λ baryon, with a scaled momentum $x_p > 0.5$. Details of the particle selections are given below. Since this high- x_p cut rejects relatively few $Z^0 \rightarrow \tau^+\tau^-$ events in our sample, we further demand at least eight good charged tracks [20] in an event. In addition, to ensure good π^\pm , K^\pm and proton separation, and reliable K_S^0

²OPAL uses a right handed coordinate system in which the z axis points along the direction of the electron beam, r is the coordinate normal to this axis, and θ and ϕ are the polar and azimuthal angles with respect to z .

and Λ reconstruction, we require that the tagging particles have a polar angle $|\cos\theta| < 0.7$. For $|\cos\theta| > 0.7$, the dE/dx separation of kaons and protons from pions degrades rapidly with increasing $|\cos\theta|$ of the tracks. In order to select events which are well contained in the detector, we restrict the polar angle of the thrust axis (calculated using both charged tracks and clusters in the electromagnetic calorimeter which have no associated track in the jet chamber) to satisfy $|\cos\theta_{\text{Thrust}}| < 0.8$. With these requirements, 198 309 events are retained. The remaining background from $Z^0 \rightarrow \tau^+\tau^-$ events in our sample is negligible (less than 0.05%), as estimated from Monte Carlo simulations.

Crucial to this analysis is the identification and separation of samples of charged pions, charged kaons and protons, which is achieved using the dE/dx measurement, and K_S^0 and Λ baryons, which are observed by reconstructing their decay vertices and calculating the invariant mass of the decay products. Efficiency losses which are common to all particle types, such as the finite geometric acceptance, etc., can be absorbed into the values of η_q^h . However, other sources, such as those due to particle identification (dE/dx , secondary vertex finding) have to be taken into account for the hadronisation symmetries. Similarly, there exists some misidentification probability leading to a migration from the true to an apparent particle identity, which is especially relevant for the stable charged particles. This must also be taken into account and the hadronisation symmetries corrected for different detection efficiencies and migrations. Due to the fundamentally different reconstruction of the weakly decaying K_S^0 and Λ , these samples are largely decoupled from the charged hadron samples. The relation between apparent particle type h_{det} and true particle type h is given by some flow matrix, $\mathcal{E}_{h_{\text{det}}}^h$, such that

$$N_{h_{\text{det}}} = \sum_h \mathcal{E}_{h_{\text{det}}}^h N_h . \quad (19)$$

Similarly, the forward-backward asymmetries for the measured samples $A_{FB}^{h_{\text{det}}}$ are related to the pure particle type asymmetries A_{FB}^h by

$$A_{FB}^{h_{\text{det}}} = \sum_h \mathcal{E}_{h_{\text{det}}}^h A_{FB}^h . \quad (20)$$

Apart from reducing the discrimination power between the various flavours, some systematic uncertainties related both to the efficiency and purity are introduced.

For the dE/dx measurement, tracks are required to have at least 20 hits in the jet chamber used in the calculation of the energy loss, a polar angle θ satisfying $|\cos\theta| < 0.7$, a distance of closest approach to the interaction point in the plane orthogonal to the beam direction of $|d_0| < 2$ mm, and the corresponding distance along the beam direction $|z_0| < 40$ cm. To suppress badly measured tracks we further restrict the scaled momentum to $x_p < 1.07$, which takes into account the 7% momentum resolution of a track with $x_p = 1$. A study of muon pair events finds that less than 0.3% of tracks which have the full beam energy have an incorrect charge assignment.

To separate samples of pions, kaons and protons, we use for each track the dE/dx weight, w_h , which is defined as the signed χ^2 probability of the track to be consistent with a certain particle species hypothesis, h . The sign represents the sign of the difference between the measured $dE/dx(\text{meas.})$ and the expected $dE/dx(\text{exp.})$ for the particle species hypothesis, namely a positive weight if $dE/dx(\text{meas.}) > dE/dx(\text{exp.})$ and a negative weight if $dE/dx(\text{meas.}) < dE/dx(\text{exp.})$. In particular, we require:

- for pion candidates: ($w_{\pi^\pm} > 0.01$ or $w_{\pi^\pm} < -0.1$), and $|w_{K^\pm}| < 0.1$;
- for kaon candidates: $|w_{K^\pm}| > 0.1$ and $|w_{\pi^\pm}| < 0.1$;
- for proton candidates: ($w_{p(\bar{p})} > 0.1$ or $w_{p(\bar{p})} < -0.01$), and $|w_{K^\pm}| < 0.1$.

These selection criteria result in three disjoint track samples. The dE/dx separation power as a function of charged track momentum is shown in Fig. 1. In addition, charged tracks are rejected if they pass either the standard electron or muon identification requirements [15,16]. After these requirements, backgrounds from electrons and muons are negligible, as determined from Monte Carlo simulations. The largest contamination is the 0.8% of pion candidates which are actually muons. In addition, some contamination from charged hyperons (mostly Σ^-) is present in the proton sample at the 10% level according to the Monte Carlo simulations. However, since we make no hadronisation assumptions about the proton sample, this contamination is not a problem for the analysis.

These cuts (including the event and thrust axis cuts) lead to efficiencies of $(34.7 \pm 0.1 \pm 5.2)\%$ for pion tagged hemispheres, $(29.5 \pm 0.1 \pm 4.6)\%$ for kaon tagged hemispheres and $(23.4 \pm 0.3 \pm 5.3)\%$ for proton tagged hemispheres, where in each case the uncertainties are statistical and systematic. The efficiency is defined as the number of event hemispheres which are tagged at the detector level divided by the number of event hemispheres which are tagged at the Monte Carlo generator level. Differences in the tagging efficiencies are due entirely to the dE/dx selections. The systematic uncertainty is determined by scaling the corresponding widths of the dE/dx distributions, σ , by 1.00 ± 0.05 and by varying the expected dE/dx value for each particle type by $\pm 0.15\sigma$. The ranges of these uncertainties come from checks with pions from $K_S^0 \rightarrow \pi^+\pi^-$ decays and protons from $\Lambda \rightarrow p\pi^-$ decays for track momenta greater than 2 GeV in which the means and widths of the normalised dE/dx distributions showed maximum deviations of $\pm 0.15\sigma$ and $\pm 5\%$, respectively. The uncertainties are therefore strongly positively correlated between the various particle species. The other selection criteria were studied in the Monte Carlo event samples and found to have no significant bias to select any one tagging particle type over another.

The procedures to identify the weakly decaying hadrons K_S^0 and Λ are described in detail in [21] and [22], respectively. Here we summarise the main ingredients. To find $K_S^0 \rightarrow \pi^+\pi^-$ and $\Lambda \rightarrow p\pi^-$ candidates, we combine two oppositely charged tracks which have at least 20 hits in the jet chamber. We then search for a crossing point of these tracks in the plane orthogonal to the beam axis. If a good secondary vertex is found, the $\pi^+\pi^-$ and $p\pi^-$ invariant masses of the combinations are calculated. Good K_S^0 candidates are required to have $x_p > 0.5$ and have invariant masses in the ranges $430 \text{ MeV} < m_{\pi^+\pi^-} < 570 \text{ MeV}$ and $m_{p\pi^-} > 1.13 \text{ GeV}$, in order to reduce the contamination from $\Lambda \rightarrow p\pi^-$ decays, where $m_{\pi^+\pi^-}$ is the invariant mass of the tracks assuming that they are a pair of pions and $m_{p\pi^-}$ a proton-pion pair. Likewise, all candidates which have $x_p > 0.5$ and $1.10 \text{ GeV} < m_{p\pi^-} < 1.13 \text{ GeV}$ are accepted as high-momentum Λ candidates. No additional rejection of $K_S^0 \rightarrow \pi^+\pi^-$ background in the Λ sample using an invariant mass cut is made since such a rejection cannot be done efficiently. The invariant mass distributions for all candidates which pass these selection criteria are shown in Figs. 2 and 3. The detection efficiencies are determined using the Monte Carlo simulated events. After correcting for mass resolution differences between data and Monte Carlo simulation as in [22], the efficiencies, defined as before, are found to be $(9.4 \pm 0.1 \pm 0.3)\%$ for K_S^0 tagged hemispheres

and $(4.7 \pm 0.1 \pm 0.3)\%$ for Λ tagged hemispheres, where the errors are statistical and systematic, respectively. The systematic errors are mainly due to uncertainties in the correction factors for the different mass resolutions in the data and Monte Carlo and the simulation of other cut distributions. Detailed treatments of the determination of these systematic errors can be found in [21, 22]. With these requirements we select the number of tagged hemispheres and double tagged events listed in Table 1.

The purities of the final samples, as determined from the efficiencies calculated above with appropriate weighting by the relative particle yields in the data are given in Table 2. Although there is some uncertainty in the particle identification efficiencies, the charged pion, kaon and proton sample purities are known to ± 0.011 , ± 0.013 and ± 0.052 , respectively. The errors are smaller for the purities than for the efficiencies because of the positive correlations among the efficiencies. The K_S^0 and Λ sample purities are largely uncorrelated with those of the charged hadron samples. In addition to small combinatorial backgrounds composed of randomly paired tracks, $K_S^0 \rightarrow \pi^+\pi^-$ decays form the principal background in the Λ sample, and $\Lambda \rightarrow p\pi^-$ combinations form a somewhat less important background in the K_S^0 sample. The total backgrounds are determined by fitting to the invariant mass spectrum shown in Fig. 2, as in [21], and by using a sideband method to determine the background in the distribution shown in Fig. 3, as in [22]. For the K_S^0 sample, after subtracting the contribution from $\Lambda \rightarrow p\pi^-$ decays, a combinatorial background level of $(5.6 \pm 2.9)\%$ is found, where the error is systematic [21]. Combining this with the relative uncertainty on the efficiency, the total relative systematic error on the K_S^0 yield is $\pm 4.1\%$. For the Λ , the combinatorial background present in the sample is $(7.7 \pm 2.4)\%$, where the error is again systematic [22]. The total relative error on the Λ yield is therefore $\pm 6.3\%$.

hadron type	tagged hemispheres	double tagged events				
		π^\pm	K^\pm	$p(\bar{p})$	K_S^0	$\Lambda(\bar{\Lambda})$
π^\pm	52 170	392	416	99	46	18
K^\pm	40 229		265	136	48	15
$p(\bar{p})$	9 350			13	15	4
K_S^0	5 026				3	1
$\Lambda(\bar{\Lambda})$	1 349					1

Table 1: Number of tagged event hemispheres and double tagged events for $x_p > 0.5$.

5 Heavy Quark Contributions

Before determining the light-flavour electroweak properties, we first find the contributions of charm and bottom quarks to the selected samples. In the case of the bottom quark, we determine the fraction directly from the data (except for the tagged Λ sample) by searching for a secondary vertex or for a lepton with a high transverse momentum relative to the jet direction in the high- x_p samples. Lack of statistics prevents a similar method from being used to determine the charm backgrounds with the necessary precision. Instead we use the JETSET model and estimate the uncertainties based on the measured production and decay properties

assigned	true π^\pm	true K^\pm	true $p(\bar{p})$	true K_S^0	true $\Lambda(\bar{\Lambda})$
π^\pm	0.895	0.080	0.002	0.011	0.000
K^\pm	0.106	0.712	0.171	0.001	0.008
$p(\bar{p})$	0.013	0.367	0.591	0.001	0.028
K_S^0	0.003	0.001	0.000	0.979	0.017
$\Lambda(\bar{\Lambda})$	0.001	0.003	0.000	0.307	0.690

Table 2: The particle composition in samples assigned as charged pions, charged and neutral kaons, protons, Λ baryons. Note that in some of the rows the numbers do not add up to 100%, due to the presence of small backgrounds from other sources such as leptons. The combinatorial backgrounds under the K_S^0 and Λ signals are not considered here and are discussed in the text. Charged hyperons were treated as “protons” for the purposes of identification.

of charmed hadrons. Due to the low statistics available, the b quark flavour fractions and reliabilities for the tagged Λ sample are also taken from the simulation.

5.1 Bottom Quark Contributions

To determine the fractions f_b^h of $Z^0 \rightarrow b\bar{b}$ events in the high- x_p event samples, we search for a secondary vertex displaced from the primary event vertex in the event hemisphere opposite to that of the high- x_p tagging particle. The details of the vertex finding are discussed in [14]. We require the vertex to have at least four assigned tracks and to have a decay length significance $l/\sigma_l > 10$, where l is the observed distance to the event vertex and σ_l its error. This yields a b tagging efficiency per event hemisphere, ϵ_b , of about 16% with a purity, P_b , of $(96 \pm 1)\%$, using the methods in [23]. The desired fractions are then given by:

$$f_b^h = \frac{1}{P_b} \frac{N_h^{\text{b-tag}}}{N_h} \left(\frac{2N_{\text{had}}R_b}{N^{\text{b-tag}}} \right) - \frac{1 - P_b}{P_b} \mathcal{B}_h \quad (21)$$

and are listed in Table 3. Here $N_h^{\text{b-tag}}$ is the observed number of events with a tagged hadron h in one hemisphere and a secondary b vertex in the one opposite and $N^{\text{b-tag}}$ is the total number of hemispheres with a secondary b vertex. The term \mathcal{B}_h takes into account the contribution to the measured fraction from events tagged as a b event but which do not come from $Z^0 \rightarrow b\bar{b}$ events. This term, which is weighted by $(1 - P_b)$, is calculated from Monte Carlo simulated events and is the only model-dependent number used in the measurement of the backgrounds from $Z^0 \rightarrow b\bar{b}$ events. A conservative error of 50% is assigned to the calculated value of \mathcal{B}_h , which for pions, for example, is calculated to be $\mathcal{B}_{\pi^\pm} = 0.127 \pm 0.015 \pm 0.064$, where the first error is statistical and the second systematic. The values for the other hadron types are similar. Given the very high purity of the b tagged sample, the influence of this term on the final measurement is small. However, other sources of systematic uncertainty, such as uncertainties in R_b and P_b , are negligible in comparison. Due to low statistics, $f_b^{\Lambda(\bar{\Lambda})}$ is taken from the simulation with a $\pm 50\%$ relative systematic error, as given in Table 3.

In order to verify that the method does not introduce systematic biases, the measurement is repeated on JETSET events with a detailed simulation of the OPAL detector and the results

are compared with the true b fractions in the Monte Carlo event sample. No systematic biases are found. The measurement is also checked with the data by selecting b events using leptons with a high transverse momentum with respect to the jet direction (described in more detail below). The two measurements are found to be in good agreement, although the statistical errors for the lepton samples are large. The dependence of the measurement on the purity of the b tagged sample is also checked by varying the minimum decay length significance over the range from 6 to 14. No systematic dependence of the measured b fractions is found.

hadron type	f_b^h	r_b^h
π^\pm	0.078 ± 0.004	0.79 ± 0.11
K^\pm	0.039 ± 0.004	0.67 ± 0.12
$p(\bar{p})$	0.051 ± 0.009	0.71 ± 0.30
K_S^0	0.036 ± 0.010	—
$\Lambda(\bar{\Lambda})$	0.031 ± 0.015	0.29 ± 0.11

Table 3: Fractions and reliabilities of hadrons from bottom events, where the errors include both statistical and systematic uncertainties added in quadrature.

To obtain the high- x_p hadron charge reliabilities in bottom events one has to know the charge of the tagged bottom hadron. Instead of secondary vertices, we therefore use high-energy muons to identify bottom particles. Details of the muon identification and tagging procedures are given in [16]. The observed charged tracks and neutral clusters in the electromagnetic calorimeter are combined into jets of a maximum observable invariant mass of 7 GeV using the JADE algorithm with the ‘E0’ recombination scheme [24]. The event is tagged as a $Z^0 \rightarrow b\bar{b}$ event if a muon candidate is found with a total momentum greater than 3 GeV and a transverse momentum with respect to the jet axis, p_T , of at least 1 GeV.

First we determine the overall charge reliability of the high- p_T muon using double tagged b events. The b reliability is given by:

$$(2r_b - 1) = \sqrt{2 \frac{N_{bb}^{\text{OPP}}}{N_{bb}} - 1}, \quad (22)$$

where N_{bb} is the total number of double tagged b events and N_{bb}^{OPP} is the number of such events in which the tagging leptons have opposite charges. We measure $r_b = 0.650 \pm 0.015$, where the error is statistical. Note that this measurement includes effects such as $B^0\bar{B}^0$ mixing. The high- x_p hadron charge reliability is then given by:

$$(2r_b^h - 1) = \frac{2N_h^{\text{b-tag,OPP}}/N_h^{\text{b-tag}} - 1}{2r_b - 1}, \quad (23)$$

where $N_h^{\text{b-tag,OPP}}$ is the number of events in $N_h^{\text{b-tag}}$ in which the tagging particles have opposite charges. The results are also listed in Table 3. Again, due to low statistics, $r_b^{\Lambda(\bar{\Lambda})}$ is taken from the simulation with a systematic error corresponding to a relative error of $\pm 50\%$ on $(2r_b^{\Lambda(\bar{\Lambda})} - 1)$, which is the factor relevant for the measurement of the forward-backward asymmetries.

5.2 Charm Quark Contributions

In the absence of an efficient enough charm tag we estimate the f_c^h from Monte Carlo simulations. The estimated uncertainties on the f_c^h are based on the knowledge of charm production and decay. The essential ingredients are the fragmentation functions of charm quarks [25] and the relative production yields of charmed hadrons [26] and their decay properties [2]. Taking into account the corresponding measurements and their uncertainties, we derive the fractions as listed in Table 4.

To cross-check these estimates with the data, we search in the tagged samples of high- x_p particles for $D^{*\pm}$ mesons in the opposite hemisphere. We use the transition $D^{*\pm} \rightarrow D^0\pi^\pm$ and the D^0 decay modes $D^0 \rightarrow K^-\pi^+$, $K^-e^+\nu_e$, and $K^-\mu^+\nu_\mu$. Details of the selection procedures are given in [27]. The results are consistent with the above estimates although with large statistical uncertainties. Results are reported for comparison in Table 4.

hadron type	f_c^h (JETSET)	f_c^h (DATA)	r_c^h (JETSET)
π^\pm	0.068 ± 0.007	0.04 ± 0.04	0.70 ± 0.12
K^\pm	0.101 ± 0.011	0.17 ± 0.06	0.25 ± 0.06
$p(\bar{p})$	0.088 ± 0.009		0.40 ± 0.12
K_S^0	0.114 ± 0.012		—
$\Lambda(\bar{\Lambda})$	0.091 ± 0.010		0.70 ± 0.12

Table 4: Fractions and reliabilities for hadrons from charm events, where the errors include both statistical and uncorrelated systematic uncertainties added in quadrature. No measurements were possible for $f_c^{p(\bar{p})}$, $f_c^{K_S^0}$, and $f_c^{\Lambda(\bar{\Lambda})}$ in the data due to lack of statistics. In addition to these uncertainties in the individual particle fractions, overall shifts between -5% and $+20\%$ are observed due to uncertainties in the charm fragmentation function and have to be taken into account.

We also take the high- x_p hadron charge reliabilities in charm events from studies of simulated events. The values are also given in Table 4. As a cross-check we measure the charge reliabilities from data using the $D^{*\pm}$ sample described above, using Eq. 23, but taking the overall charm reliability r_c from simulation. The results are compatible with the values from the simulation but have large statistical errors.

Several sources of systematic uncertainties have been considered. Of particular relevance are those affecting the relative fractions of K_S^0 and K^\pm from charm decays. The ratio of K_S^0 to K^\pm production depends on the inclusive branching ratios of the D^0 , D^\pm , D_s and Λ_c^+ into the tagged particle species and the corresponding decay multiplicities. The former were taken from [2] and propagated through to the f_c^h . The decay multiplicities as used in the JETSET simulation were compared to the measurements of the Mark III collaboration [28]. The differences lead to uncertainties of $\sim 4\%$ for each particle species. The resulting errors for each of them are given in Table 4. In addition, the f_c^h of all hadron species are affected coherently by the hardness of the fragmentation function. Allowing the ϵ_c parameter of the Peterson et al. fragmentation function [29] to vary between $0.020 \leq \epsilon_c \leq 0.039$, which corresponds to $0.474 \leq \langle x_E^D \rangle \leq 0.501$, as given by the measurements of the D^* and D fragmentation functions [25], overall changes of -5% to $+20\%$ are introduced.

6 The Branching Fractions and Forward-Backward Asymmetries of Light Flavours

As discussed in Section 2 the branching fractions of the Z^0 into light quarks and the forward-backward asymmetries are determined under the assumption that the electroweak couplings for down and strange quarks are the same. We start with the branching fractions and afterwards discuss the forward-backward asymmetries in Section 6.2, considering at first only statistical uncertainties. The systematic uncertainties are addressed in Section 7.

6.1 The Branching Fractions R'_q

After subtracting the contributions from heavy quarks, we solve the equation system for $R_{d,s}$. In addition to the five measured numbers of tagged hemispheres and fifteen combinations of double tagged events (Eqs. 1–2), we use the five hadronisation symmetries (Eqs. 4–8). Therefore, there are twenty measurements and twelve unknown parameters, including $R_{d,s}$, a global ρ , and ten η_q^h . The equation system is solved by minimising a χ^2 function which uses the 20 measured quantities of Eqs. 1–2. In order to minimise the dependence of our results on heavy flavour electroweak measurements, we determine the partial light flavour branching fractions:

$$R'_{d,s} = 0.371 \pm 0.016, \tag{24}$$

where the error is purely statistical and the value of χ^2 is 4.4 for eight degrees of freedom at the minimum. The result for $R'_u = 0.258 \pm 0.031$ is fully anticorrelated to the value of $R'_{d,s}$ since $R'_d + R'_u + R'_s = 1$. The solution is tested for stability and uniqueness by using different starting values for the unknown parameters. No other physical solution is found. The Standard Model expectations for a top quark mass of 175 GeV and a Higgs boson mass of 300 GeV are 0.359 and 0.282, respectively, consistent with the above measurements. If we use the world average values for R_c and R_b [2], we can determine the branching fraction of the Z^0 into down-type light quarks:

$$R_{d,s} = 0.230 \pm 0.010, \tag{25}$$

where again the error is purely statistical. The corresponding $R_u = 0.160 \pm 0.019$ is fully anticorrelated with this result.

The values for the other parameters are given in Table 5, along with those obtained from the solution using Monte Carlo events for comparison. Some differences are found for $\eta_d^{\pi^\pm}$ and for the baryons. The value of the hemisphere correlation, ρ , is comparable in data and Monte Carlo. Most of the correlation is due to the limited geometric acceptance and the selection criteria, which are well modelled in the Monte Carlo simulations. The correlation in JETSET events without detector simulation and without any restrictions on the geometric acceptance is about 1.07 and is due to hemisphere correlations from gluon radiation [6].

parameter	OPAL	JETSET	(input)
ρ	$1.290 \pm 0.043 \pm 0.025$	1.286 ± 0.032	(1.238)
$\eta_d^{\pi^\pm}$	$0.0406 \pm 0.0016 \pm 0.0021$	0.0441 ± 0.0012	(0.0438)
$\eta_s^{\pi^\pm}$	$0.0074 \pm 0.0028 \pm 0.0011$	0.0084 ± 0.0021	(0.0089)
$\eta_d^{K^\pm}$	$0.0010 \pm 0.0052 \pm 0.0012$	0.0038 ± 0.0024	(0.0045)
$\eta_u^{K^\pm}$	$0.0230 \pm 0.0052 \pm 0.0011$	0.0178 ± 0.0025	(0.0112)
$\eta_s^{K^\pm}$	$0.0344 \pm 0.0029 \pm 0.0013$	0.0363 ± 0.0027	(0.0407)
$\eta_d^{p(\bar{p})}$	$0.0006 \pm 0.0027 \pm 0.0008$	0.0065 ± 0.0032	(0.0042)
$\eta_u^{p(\bar{p})}$	$0.0082 \pm 0.0056 \pm 0.0015$	0.0086 ± 0.0048	(0.0124)
$\eta_s^{p(\bar{p})}$	$0.0086 \pm 0.0023 \pm 0.0005$	0.0042 ± 0.0017	(0.0037)
$\eta_d^{\Lambda(\bar{\Lambda})}$	$0.0049 \pm 0.0020 \pm 0.0004$	0.0032 ± 0.0014	(0.0022)
$\eta_s^{\Lambda(\bar{\Lambda})}$	$0.0040 \pm 0.0033 \pm 0.0005$	0.0107 ± 0.0024	(0.0129)

Table 5: Free parameters in the equation system and their fitted values, with statistical and systematic errors, which are highly correlated. Also given for comparison are the values from a solution using JETSET events with full detector simulation with statistical errors only and the input values given in parentheses. Good agreement between the Monte Carlo input values and solutions is found.

6.2 The Forward-Backward Asymmetries

To determine the forward-backward asymmetries, we divide the data sample into events collected within ± 200 MeV of the Z^0 peak with an average centre-of-mass energy $\langle E_{\text{cm}} \rangle = 91.2$ GeV, and those below and above the peak, which have average centre-of-mass energies of $\langle E_{\text{cm}} \rangle = 89.5$ GeV and $\langle E_{\text{cm}} \rangle = 92.9$ GeV, respectively. The backgrounds due to charm and bottom events are known since the heavy flavour terms in Eq. 12 have been measured separately³. We then use Eq. 12 together with the relation of Eq. 13 to determine the reliabilities of the charge tags for the light flavours. The measured hadron forward-backward asymmetries, which have been determined by maximising a log-likelihood function, are listed in Table 6.

hadron type	$E_{\text{cm}} < m_{Z^0}$	$E_{\text{cm}} \sim m_{Z^0}$	$E_{\text{cm}} > m_{Z^0}$
π^\pm	$(-1.22 \pm 2.14) \times 10^{-2}$	$(-1.60 \pm 0.52) \times 10^{-2}$	$(+0.12 \pm 1.78) \times 10^{-2}$
K^\pm	$(+1.76 \pm 2.52) \times 10^{-2}$	$(-3.12 \pm 0.58) \times 10^{-2}$	$(-6.66 \pm 2.04) \times 10^{-2}$
$p(\bar{p})$	$(+9.98 \pm 5.18) \times 10^{-2}$	$(-1.28 \pm 1.26) \times 10^{-2}$	$(+3.42 \pm 4.42) \times 10^{-2}$
$\Lambda(\bar{\Lambda})$	$(+10.0 \pm 12.8) \times 10^{-2}$	$(+4.32 \pm 3.18) \times 10^{-2}$	$(+8.8 \pm 11.4) \times 10^{-2}$

Table 6: The measured forward-backward asymmetries, $A_{FB}^{h_{\text{det}}}$, with statistical errors for various centre-of-mass energies, E_{cm} . Note that the $A_{FB}^{h_{\text{det}}}$ have not been corrected for the purities of identified samples. Results are given in percent.

We extend the assumption $R_d = R_s$ to the equality of the forward-backward asymmetries of down and strange quarks, and use the hadronisation symmetries of Eqs. 14–16 and the

³See Tables 3-4 for the heavy flavour fractions f_q^h and reliabilities r_q^h , and [2] for $A_{FB}(c)$ and $A_{FB}(b)$.

constraint from Eq. 17. This leaves 8 unknown reliabilities, 10 combinations of double tagged events of same and opposite charges (note that double tagged events with K_S^0 cannot be used), and 4 measured hadron $A_{FB}^{h_{\text{det}}}$ with which to determine the light flavour forward-backward asymmetries. We find for energies near the Z^0 peak:

$$A_{FB}(d,s) = 0.068 \pm 0.035 \quad \text{and} \quad A_{FB}(u) = 0.040 \pm 0.067, \quad (26)$$

where the errors given are statistical only. The correlation between these results is +91%. The reliabilities are found to be consistent with the JETSET predictions, although with large statistical errors. The three best measured reliabilities are $r_d^{\pi^\pm} = 0.81 \pm 0.02$, $r_u^{K^\pm} = 0.70 \pm 0.18$, and $r_s^{K^\pm} = 1.05 \pm 0.06$, where the errors are statistical. Near the Z^0 peak, the flavour composition changes very slowly and QCD scaling violations are likewise negligible. This is consistent with results from studies using JETSET where the flavour fractions and reliabilities for the off-peak data are found to be the same as for the on-peak data. Therefore, we use the flavour fractions and reliabilities as determined from the on-peak data to determine the off-peak forward-backward asymmetries. We find for energies above the Z^0 peak:

$$A_{FB}(d,s) = 0.228 \pm 0.082 \quad \text{and} \quad A_{FB}(u) = 0.397 \pm 0.183, \quad (27)$$

and below the Z^0 peak:

$$A_{FB}(d,s) = 0.019 \pm 0.098, \quad \text{and} \quad A_{FB}(u) = 0.103 \pm 0.216. \quad (28)$$

The values as a function of the centre-of-mass energy are shown in Fig. 4, along with the predictions of the Standard Model, which are found to be consistent with the data within the statistical errors. The systematic errors are discussed in the following section.

7 Systematic Uncertainties

The procedure used in this paper is tested with approximately eight million hadronic Z^0 decays generated with the JETSET model and passed through a detailed simulation of the OPAL detector. The results obtained from the fit, to the reconstructed events, $R_{d,s} = 0.224 \pm 0.008$ and $A_{FB}(d,s) = 0.128 \pm 0.025$, where the errors are statistical only, are found to be in agreement with the input values for $R_{d,s} = 0.220$ and $A_{FB}(d,s) = 0.100$.

Several sources of systematic uncertainty affect our result. They can be divided into three classes: 1) those due to detector effects, 2) those due to model assumptions, and 3) uncertainties in the heavy quark contributions. Since these three classes of errors are largely uncorrelated, we estimate their individual impact on the branching fractions and asymmetries and add them quadratically to obtain the overall systematic error. The individual systematic errors on the electroweak observables are summarised in Table 7 for $R_{d,s}$ and in Table 8 for the forward-backward asymmetries. The errors are determined by changing each input parameter in turn, repeating the analysis, and observing the shifts in the results, as given in the tables.

Source of Error	$\delta R'_{d,s}$	$\delta R_{d,s}$
dE/dx resolution $\pm 5\%$	∓ 0.0037	∓ 0.0023
dE/dx mean $\pm 0.15 \sigma$	± 0.0016	± 0.0010
K_S^0 purity and efficiency $\pm 4.1\%$	∓ 0.0124	∓ 0.0077
Λ purity and efficiency $\pm 6.3\%$	± 0.0003	± 0.0002
$\eta_u^{\pi^\pm} / \eta_d^{\pi^\pm} = 1.00 \pm 0.02$	< 0.0001	< 0.0001
$\eta_d^{K^0(\bar{K}^0)} / \eta_u^{K^\pm}, \eta_u^{K^0(\bar{K}^0)} / \eta_d^{K^\pm} = 1.00 \pm 0.02$	∓ 0.0039	∓ 0.0024
$\eta_s^{K^0(\bar{K}^0)} / \eta_s^{K^\pm} = 1.00 \pm 0.02$	∓ 0.0022	∓ 0.0014
$\eta_u^{\Lambda(\bar{\Lambda})} / \eta_d^{\Lambda(\bar{\Lambda})} = 1.00 \pm 0.02$	∓ 0.0002	∓ 0.0001
$\rho(\text{baryon}) = \rho \times (1.00 \pm 0.02)$	∓ 0.0021	∓ 0.0013
$f_c^{\pi^\pm} = 0.068 \pm 0.007$	∓ 0.0005	∓ 0.0003
$f_c^{K^\pm} = 0.101 \pm 0.011$	± 0.0050	± 0.0031
$f_c^{P(\bar{P})} = 0.088 \pm 0.009$	∓ 0.0011	∓ 0.0007
$f_c^{K_S^0} = 0.114 \pm 0.012$	∓ 0.0042	∓ 0.0026
$f_c^{\Lambda(\bar{\Lambda})} = 0.091 \pm 0.010$	< 0.0001	< 0.0001
$0.020 \leq \epsilon_c \leq 0.039$	± 0.0015	± 0.0009
$f_b^{\pi^\pm} = 0.078 \pm 0.004$	∓ 0.0003	∓ 0.0002
$f_b^{K^\pm} = 0.039 \pm 0.004$	± 0.0016	± 0.0010
$f_b^{P(\bar{P})} = 0.051 \pm 0.009$	∓ 0.0011	∓ 0.0007
$f_b^{K_S^0} = 0.036 \pm 0.010$	∓ 0.0033	∓ 0.0021
$f_b^{\Lambda(\bar{\Lambda})} = 0.031 \pm 0.015$	± 0.0002	± 0.0001
Sub-total Systematic Error	0.0160	0.0097
$R_c = 0.158 \pm 0.010$	< 0.0001	∓ 0.0037
$R_b = 0.2212 \pm 0.0019$	< 0.0001	∓ 0.0008
Total Systematic Error	0.0160	0.0104
Total Statistical Error	0.0155	0.0096
Total Error	0.0223	0.0141

Table 7: Sources of systematic error and their effects on the measurement of $R'_{d,s}$ and $R_{d,s}$. The corresponding errors on R'_u and R_u are twice those of $R'_{d,s}$ and $R_{d,s}$ and are negatively correlated, with the exception of the uncertainties due to R_c and R_b , which are positively correlated.

Source of Error	$\delta A_{FB}(d, s)$	$\delta A_{FB}(u)$
dE/dx resolution $\pm 5\%$	∓ 0.0018	∓ 0.0032
dE/dx mean $\pm 0.15 \sigma$	± 0.0009	± 0.0025
K_S^0 purity and efficiency $\pm 4.1\%$	∓ 0.0051	∓ 0.0152
Λ purity and efficiency $\pm 6.3\%$	± 0.0002	± 0.0006
$r_d^{K^\pm} = 0.20 \pm 0.10$	∓ 0.0009	∓ 0.0013
$r_u^{\pi^\pm}/r_d^{\pi^\pm} = 1.00 \pm 0.05$	∓ 0.0027	∓ 0.0072
$r_s^{\pi^\pm} = 0.50 \pm 0.05$	∓ 0.0014	∓ 0.0010
$r_u^{\Lambda(\bar{\Lambda})}/r_d^{\Lambda(\bar{\Lambda})} = 1.00 \pm 0.05$	∓ 0.0013	∓ 0.0024
$\rho(\text{baryon}) = \rho \times (1.00 \pm 0.02)$	∓ 0.0032	∓ 0.0059
$f_c^{\pi^\pm} = 0.068 \pm 0.007$	± 0.0003	∓ 0.0012
$f_c^{K^\pm} = 0.101 \pm 0.011$	∓ 0.0009	± 0.0020
$f_c^{p(\bar{p})} = 0.088 \pm 0.009$	± 0.0004	∓ 0.0003
$f_c^{K_S^0} = 0.114 \pm 0.012$	∓ 0.0012	∓ 0.0046
$f_c^{\Lambda(\bar{\Lambda})} = 0.091 \pm 0.010$	< 0.0001	± 0.0002
$0.020 \leq \epsilon_c \leq 0.039$	∓ 0.0022	∓ 0.0045
$r_c^{\pi^\pm} = 0.70 \pm 0.12$	∓ 0.0012	∓ 0.0087
$r_c^{K^\pm} = 0.25 \pm 0.06$	± 0.0026	± 0.0044
$r_c^{p(\bar{p})} = 0.40 \pm 0.12$	∓ 0.0018	∓ 0.0033
$r_c^{\Lambda(\bar{\Lambda})} = 0.70 \pm 0.12$	∓ 0.0002	∓ 0.0002
$f_b^{\pi^\pm} = 0.078 \pm 0.004$	± 0.0008	± 0.0020
$f_b^{K^\pm} = 0.039 \pm 0.004$	∓ 0.0007	± 0.0001
$f_b^{p(\bar{p})} = 0.051 \pm 0.009$	± 0.0009	± 0.0007
$f_b^{K_S^0} = 0.036 \pm 0.010$	∓ 0.0009	∓ 0.0036
$f_b^{\Lambda(\bar{\Lambda})} = 0.031 \pm 0.015$	± 0.0001	± 0.0003
$r_b^{\pi^\pm} = 0.79 \pm 0.11$	± 0.0030	± 0.0129
$r_b^{K^\pm} = 0.67 \pm 0.12$	∓ 0.0039	∓ 0.0062
$r_b^{p(\bar{p})} = 0.71 \pm 0.30$	± 0.0047	± 0.0078
$r_b^{\Lambda(\bar{\Lambda})} = 0.29 \pm 0.11$	< 0.0001	< 0.0001
$R_c = 0.158 \pm 0.010$	< 0.0001	< 0.0001
$R_b = 0.2212 \pm 0.0019$	< 0.0001	< 0.0001
$A_{FB}(c) = 0.0722 \pm 0.0067$	∓ 0.0011	∓ 0.0031
$A_{FB}(b) = 0.0992 \pm 0.0035$	± 0.0001	± 0.0010
Total Systematic Error	0.0110	0.0281
Total Statistical Error	0.0342	0.0667
Total Error	0.0359	0.0723

Table 8: Sources of systematic error and their effects on the measurements of the forward-backward asymmetries for $E_{\text{cm}} \sim m_{Z^0}$.

The following systematic uncertainties are considered:

- Detector sources:
 - **hadron identification by dE/dx :** As mentioned in Section 3, we apply corrections to the apparent charged pion, charged kaon, and proton yields to take into account the migration of the true to the apparent particle species and their relative efficiencies. The uncertainties in these corrections are estimated by varying the widths, σ , of the ionisation loss distributions by $\pm 5\%$ and the central values by $\pm 0.15\sigma$. Since such changes affect all charged particle species similarly, they result in smaller uncertainties in the purities of the identified samples than the overall π^\pm , K^\pm , and proton (antiproton) identification efficiencies.
 - **efficiencies of K_S^0 and Λ :** The limited knowledge of the K_S^0 and Λ efficiencies and purities affects the discrimination power between up and down type quarks. The K_S^0 efficiency is one of the largest sources of systematic uncertainty since the difference between K_S^0 and K^\pm production separates u and d quark events, since K_S^0 tags primarily d and s quarks while K^\pm tags primarily u and s quarks.
 - **other selection criteria:** To cross-check for possible biases, we repeat the analysis with different maximum polar angles of the tagging particles between $0.6 < |\cos\theta| < 0.7$, different cuts on the polar angle of the thrust axis $0.7 < |\cos\theta_{\text{Thrust}}| < 0.9$, and different minimum values of $0.4 < x_p < 0.6$. No significant deviations are observed. Of the different minimum values of x_p which were studied, a minimum tagging hadron momentum $x_p > 0.5$ was found to result in the smallest combined error. The statistical error grows with increasing x_p , while the heavy flavour backgrounds (the uncertainty of which is a major source of systematic error) decrease. The measurements made using different minimum x_p give consistent results.
- Model uncertainties were addressed in some detail in [6]. Here we summarise the important issues:
 - **hadronisation symmetries (Eqs. 4–8):** The hadronisation relations of Eqs. 4–8 are stable against variations of fragmentation parameters within 2%. As shown in Table 7, the corresponding uncertainties in the branching fractions are small. To estimate the uncertainties in the hadronisation relations, we vary several of the important fragmentation parameters in JETSET⁴. The default values are obtained from a fit to event properties such as charged particle multiplicity, the x_p distributions for π^\pm , K^\pm , and protons, particle production rates, thrust (and other event shape) distributions [18], etc. Uncertainties in the parameters can be estimated from the corresponding increase of the χ^2 of the model with respect to the data. Requiring a change of at least $\Delta\chi^2=1$, we vary the following parameters:
 - * the hardness of the fragmentation, achieved by varying the ‘b’ parameter of the LUND symmetric fragmentation function [30] between 0.22 and 0.62,
 - * the fraction of strange quarks in the sea, by varying the relevant JETSET parameter γ_s between 0.27 and 0.36,

⁴An alternative hadronisation model is implemented in the HERWIG [31] generator. However, this model is in general not SU(2) isospin symmetric due to technical reasons [32]. Therefore, HERWIG is not suited for a general study of these hadronisation relations.

- * the fraction of vector mesons, varied between 0.4 and 0.7 for hadrons with only up and down quarks and between 0.2 and 0.6 for those containing strange quarks,
- * the production rates of tensor mesons by varying PARJ(11) between 0.4 and 0.7, PARJ(12) between 0.2 and 0.6, and switching on tensor meson production,
- * the value of Λ_{QCD} used in JETSET between 0.25 and 0.29.

The hadronisation symmetries show no statistically significant variations outside the $\pm 2\%$ range.

The relations are also confirmed by a study with the COJETS model [33] which invokes independent fragmentation.

- **hemisphere correlations:** Dynamic correlations and geometrical effects are taken into account by the ρ parameter, which is found to be independent of the primary quark flavour and the tagging hadron type to good accuracy in JETSET. To study possible breaking of this universality, we allow ρ for the proton and the Λ to vary by $\pm 2\%$ relative to the overall ρ , thus allowing for possible differences between baryon and meson hadronisation.
- Heavy flavour contributions:
 - **heavy flavour fractions and reliabilities:** The estimation of the heavy flavour contributions was discussed in Section 4. The largest uncertainties are due to the relative amounts of charged and neutral kaons from charm events. The measured D^0 and $D^\pm \rightarrow K_S^0 X$ vs. $K^\pm X$ branching fractions cause the largest systematic uncertainties, as can be seen in Tables 7 and 8. It is again the uncertainty in the ability to separate up and down quarks with charged and neutral kaons which limits the accuracy of the measurements.
 - **heavy flavour Standard Model quantities:** Variations of the heavy flavour branching fractions of the Z^0 and the forward-backward asymmetries are studied and found to have only small effects on the measurements of the light flavour electroweak parameters (see Tables 7 and 8). Note that the uncertainties on R_c and R_b have a negligible effect on the measurements of R'_q .

8 Results and Conclusions

Taking into account the systematic uncertainties, the final results (assuming $R'_d = R'_s$) are:

$$R'_{d,s} = 0.371 \pm 0.016 \text{ (stat.)} \pm 0.016 \text{ (syst.)} \quad \text{and} \quad (29)$$

$$R'_u = 0.258 \pm 0.031 \text{ (stat.)} \pm 0.032 \text{ (syst.)} . \quad (30)$$

The Standard Model predictions are 0.359 and 0.282, respectively. The R'_q have the advantage of being largely independent of R_c and R_b . If we assume the world average values of R_c and R_b from [2], we find:

$$R_{d,s} = 0.230 \pm 0.010 \text{ (stat.)} \pm 0.010 \text{ (syst.)} \quad \text{and} \quad (31)$$

$$R_u = 0.160 \pm 0.019 \text{ (stat.)} \pm 0.019 \text{ (syst.)} . \quad (32)$$

For the forward-backward asymmetries, we determine:

$$A_{FB}(d, s) = 0.068 \pm 0.035 \text{ (stat.)} \pm 0.011 \text{ (syst.)} \quad \text{and} \quad (33)$$

$$A_{FB}(u) = 0.040 \pm 0.067 \text{ (stat.)} \pm 0.028 \text{ (syst.)} \quad (34)$$

for centre-of-mass energies near the Z^0 peak. The measurement of $A_{FB}(d, s)$ is consistent with the result obtained by the DELPHI collaboration [5] using a different method which is more dependent on hadronisation models. Note that the measurements $R'_{d,s}$ and R'_u are completely negatively correlated and those of $A_{FB}(d, s)$ and $A_{FB}(u)$ more than 90% positively correlated. All of the measurements are in agreement with the predictions of the Standard Model.

We interpret these results in terms of right and left handed $Z^0 q\bar{q}$ couplings $g_R^{d,s}$ and $g_L^{d,s}$ of down and strange quarks. Here $g_L^q = \rho_q(I_3^q - e_q \sin^2 \theta_{\text{eff}})$ and $g_R^q = -\rho_q e_q \sin^2 \theta_{\text{eff}}$, ρ_q and $\sin^2 \theta_{\text{eff}}$ being the effective electroweak parameters, I_3 the third component of the weak isospin, and e_q the quark electric charge in units of the magnitude of the electron charge. The left and right handed couplings are obtained by solving the equations

$$R'_{d,s} = \frac{(g_R^{d,s})^2 + (g_L^{d,s})^2}{2[(g_R^{d,s})^2 + (g_L^{d,s})^2] + (g_R^u)^2 + (g_L^u)^2} \quad (35)$$

$$A_{FB}(d, s)(m_{Z^0}) = \frac{3}{4} \mathcal{A}_e \frac{(g_R^{d,s})^2 - (g_L^{d,s})^2}{(g_R^{d,s})^2 + (g_L^{d,s})^2} \quad (36)$$

with the electron coupling $\mathcal{A}_e = 0.1466 \pm 0.0033$ [2]. The right and left handed couplings of up quarks are assumed to be fully anticorrelated to the down/strange ones such that the denominator of Eq. 35 is equal to the Standard Model expectation. In addition, the energy dependence of the off-peak asymmetries to lowest order was parametrised according to [34]:

$$A_{FB}(s) = \frac{3 G_3(s)}{4 G_1(s)} \quad (37)$$

$$G_1(s) = Q_e^2 Q_f^2 |\chi_\gamma|^2 + 2 Q_e Q_f v_e v_f \text{Re}(\chi_\gamma^* \chi_{Z^0}) + (v_e^2 + a_e^2)(v_f^2 + a_f^2) |\chi_{Z^0}|^2 \quad (38)$$

$$G_3(s) = 2 Q_e Q_f a_e a_f \text{Re}(\chi_\gamma^* \chi_{Z^0}) + 4 v_e a_e v_f a_f |\chi_{Z^0}|^2 \quad (39)$$

with

$$\chi_{Z^0} = \frac{s}{s - m_{Z^0}^2 + i \Gamma_{Z^0} s / m_{Z^0}} \quad (40)$$

and

$$\chi_\gamma = \frac{1}{1 + \Pi_\gamma}, \quad \Pi_\gamma = -0.0593 \pm 0.0007. \quad (41)$$

The axial and vector couplings are related to the left and right handed couplings through $a_f = g_L^f - g_R^f$ and $v_f = g_L^f + g_R^f$. The values of the axial and vector couplings for the electron are taken from [2].

The measurements are corrected for initial photon radiation and QCD effects using the JETSET model [9] including initial state photon radiation. Both hard gluon and photon emission are suppressed due to the requirement of a high- x_p particle. The corrections are negligible for the measurements of R_q and for the asymmetries amount to +0.002 due to QCD effects and +0.004, +0.002 and +0.017 due to initial state photon emission at centre-of-mass

energies of 89.6, 91.2 and 92.9 GeV, respectively, which are small compared to the statistical error.

We find $g_L^{d,s} = -0.44_{-0.09}^{+0.13}$ and $g_R^{d,s} = 0.13_{-0.17}^{+0.15}$ in agreement with the Standard Model values of -0.424 and $+0.077$, respectively. The results are shown in Fig. 5 together with various confidence level regions. The fit yields a χ^2 of 2.6 for two degrees of freedom. The couplings enter quadratically into the on-peak observables but linearly in the γ - Z^0 interference contribution for the off-peak asymmetries. Therefore, only the latter measurements allow discrimination between the possible signs of g_L and g_R . The solution for a negative g_R leads to an acceptable $\chi^2=3.0$ and cannot be excluded. Solutions with a positive g_L are disfavoured and can be excluded with 76% and 83% confidence levels for negative and positive g_R , respectively.

Whereas results on down quarks exist from lepton-nucleon scattering, the present analysis is the most direct measurement of the strange quark couplings. Departing from the assumption of the equality of the couplings of down and strange quarks, we fix R'_d and determine R'_s , yielding the results presented in Fig. 6. Fixing R'_d to the Standard Model value results in $R'_s = 0.392 \pm 0.043$ (stat.) ± 0.045 (syst.). The dependence of R'_s on R'_d is linear and can be parametrised as $dR'_s/dR'_d = -1.83$. Note that the value of R'_u is completely anticorrelated to R'_s . Similar results can be obtained for $A_{FB}(s)$ and $A_{FB}(u)$ for various fixed values of $A_{FB}(d)$ as shown in Fig. 7. For $A_{FB}(d)$ fixed to the Standard Model value of 0.100, we find $A_{FB}(s) = 0.075 \pm 0.028$ (stat.) ± 0.008 (syst.) and $A_{FB}(u) = 0.086 \pm 0.030$ (stat.) ± 0.021 (syst.)%. In this case, $A_{FB}(s)$ and $A_{FB}(u)$ are only +31% correlated. Again, the dependence of the results on $A_{FB}(d)$ is linear and can be parametrised by $dA_{FB}(s)/dA_{FB}(d) = +0.32$ and $dA_{FB}(u)/dA_{FB}(d) = +1.42$. The statistical and systematic errors on $A_{FB}(u)$ are independent of $A_{FB}(d)$, while those of $A_{FB}(s)$ scale linearly with the value of $A_{FB}(s)$ such that the relative error is constant.

A measurement of all of the individual light-flavour electroweak parameters would require that the number of unknown flavour tagging efficiencies, η_q^h , be reduced. This might be possible in the future by using additional hadronisation symmetries [6] which, however, may introduce a greater model dependence.

Acknowledgements:

We particularly wish to thank the SL Division for the efficient operation of the LEP accelerator and for their continuing close cooperation with our experimental group. We thank our colleagues from CEA, DAPNIA/SPP, CE-Saclay for their efforts over the years on the time-of-flight and trigger systems which we continue to use. In addition to the support staff at our own institutions we are pleased to acknowledge the
 Department of Energy, USA,
 National Science Foundation, USA,
 Particle Physics and Astronomy Research Council, UK,
 Natural Sciences and Engineering Research Council, Canada,
 Israel Science Foundation, administered by the Israel Academy of Science and Humanities,
 Minerva Gesellschaft,
 Benozio Center for High Energy Physics,
 Japanese Ministry of Education, Science and Culture (the Monbusho) and a grant under the Monbusho International Science Research Program,

German Israeli Bi-national Science Foundation (GIF),
Direction des Sciences de la Matière du Commissariat à l'Énergie Atomique, France,
Bundesministerium für Bildung, Wissenschaft, Forschung und Technologie, Germany,
National Research Council of Canada,
Hungarian Foundation for Scientific Research, OTKA T-016660, T023793 and OTKA F-023259.

References

- [1] S.L. Glashow, J. Iliopoulos, and L. Maiani, Phys. Rev. D2 (1970) 1285;
S. Weinberg, Phys. Rev. Lett. 19 (1967) 1264;
A. Salam, *Elementary Particle Theory*, Ed. N. Svartholm (Almquist and Wiksells, Stockholm, 1969) pp. 367.
Numerical predictions of the Standard Model were calculated using ZFITTER, which is documented in:
D. Bardin et al., *ZFITTER: An Analytical Program for Fermion Pair Production in e^+e^- Annihilation*, CERN-TH.6443/92.
- [2] Particle Data Group, R.M. Barnett et al., Phys. Rev. D54 (1996) 1.
- [3] A summary of the experimental results from lepton - nucleon scattering and atomic parity violation experiments can be found in: *Precision Tests of the Standard Electroweak Model*, Ed. P. Langacker, (World Scientific, Singapore, 1994).
- [4] P. Mättig and W. Zeuner, Z. Phys. C52 (1991) 31;
OPAL Collab., P.D. Acton et al., Z. Phys. C58 (1993) 405.
L3 Collab., O. Adriani, Phys. Lett. B301 (1993) 136.
DELPHI Collab., P. Abreu et al., Z. Phys. C69 (1995) 1.
- [5] DELPHI Collab., P. Abreu et al., Z. Phys. C67 (1995) 1.
- [6] J. Letts and P. Mättig, Z. Phys. C73 (1997) 217.
- [7] Summary of experiments at PETRA, PEP, and CESR in:
P. Mättig, Phys. Rep. 177 (1989) 141.
- [8] See for example:
OPAL Collab., K. Ackerstaff et al., Z. Phys. C74 (1997) 1.
- [9] T Sjöstrand, Comp. Phys. Comm. 39 (1986) 347;
T Sjöstrand and M. Bengtsson, Comp. Phys. Comm. 43 (1987) 367;
T. Sjöstrand, Comp. Phys. Comm. 82 (1994) 74.
- [10] OPAL Collab., K. Ahmet et al., Nucl. Instr. and Meth. A305 (1991) 275.
- [11] P. Allport et al., Nucl. Instr. and Meth. A324 (1993) 34;
P. Allport et al., Nucl. Instr. and Meth. A346 (1994) 476.
- [12] M. Hauschild et al., Nucl. Instr. and Meth. A314 (1992) 74.
- [13] OPAL Collab., R. Akers et al., Z. Phys. C63 (1994) 181.
- [14] OPAL Collab., R. Akers et al., Z. Phys. C66 (1995) 19.
- [15] OPAL Collab., P.D. Acton et al., Z. Phys. C60 (1993) 19;
OPAL Collab., R. Akers et al., Z. Phys. C60 (1993) 199.
- [16] OPAL Collab., P.D. Acton et al., Z. Phys. C58 (1993) 523.

- [17] J. Allison et al., Nucl. Instr. and Meth. A317 (1992) 47.
- [18] OPAL Collab., P.D. Acton et al., Z. Phys. C58 (1993) 387;
OPAL Collab., R. Akers et al., Z. Phys. C69 (1996) 543.
- [19] OPAL Collab., G. Alexander et al., Z. Phys. C52 (1991) 175.
- [20] OPAL Collab., M.Z. Akrawy et al., Phys. Lett. B253 (1991) 511.
- [21] OPAL Collab., R. Akers et al., Z. Phys. C67 (1995) 389.
- [22] See Λ finding method #2 in:
OPAL Collab., P.D. Acton et al., Phys. Lett. B291 (1992) 503;
OPAL Collab., G. Alexander et al., Z. Phys C73 (1997) 569.
- [23] OPAL Collab., R. Akers et al., Z. Phys. C67 (1995) 365.
- [24] JADE Collab., W. Bartel et al., Z. Phys. C33 (1986) 23;
JADE Collab., S. Bethke et al., Phys. Lett. B213 (1988) 235;
OPAL Collab., M.Z. Akrawy et al., Z. Phys. C49 (1991) 375.
- [25] OPAL Collab., G. Alexander et al., Z. Phys. C72 (1996) 1.
- [26] OPAL Collab., R. Akers et al., Z. Phys. C67 (1995) 27;
OPAL Collab., R. Akers et al., Z. Phys. C67 (1995) 57.
- [27] OPAL Collab., R. Akers et al. Z. Phys. C60 (1993) 601.
- [28] Mark III Collab., D. Coffman et al., Phys. Lett. B263 (1991) 135.
- [29] C.Peterson et al., Phys. Rev. D27 (1983) 105.
- [30] B. Andersson, G. Gustafson, and B. Soderberg, Z. Phys. C20 (1983) 317.
- [31] G. Marchesini et al., Comp. Phys. Comm. 67 (1992) 465.
- [32] T. Sjöstrand, *QCD Generators*, in *Z Physics at LEP 1*, ed. G. Altarelli, R. Kleiss and C. Verzegnassi, CERN 89-08 (1989), Vol. 3, p. 250, and M. Seymour, private communication.
- [33] R. Odorico, Comp. Phys. Comm. 72 (1992) 238;
P. Mazzani and R. Odorico, Nucl. Phys. B394 (1993) 267.
- [34] M. Böhm and W. Hollik, in *Z Physics at LEP 1*, ed. G. Altarelli, R. Kleiss and C. Verzegnassi, CERN 89-08, Vol. 1, p. 203, and W. Hollik, private communication.

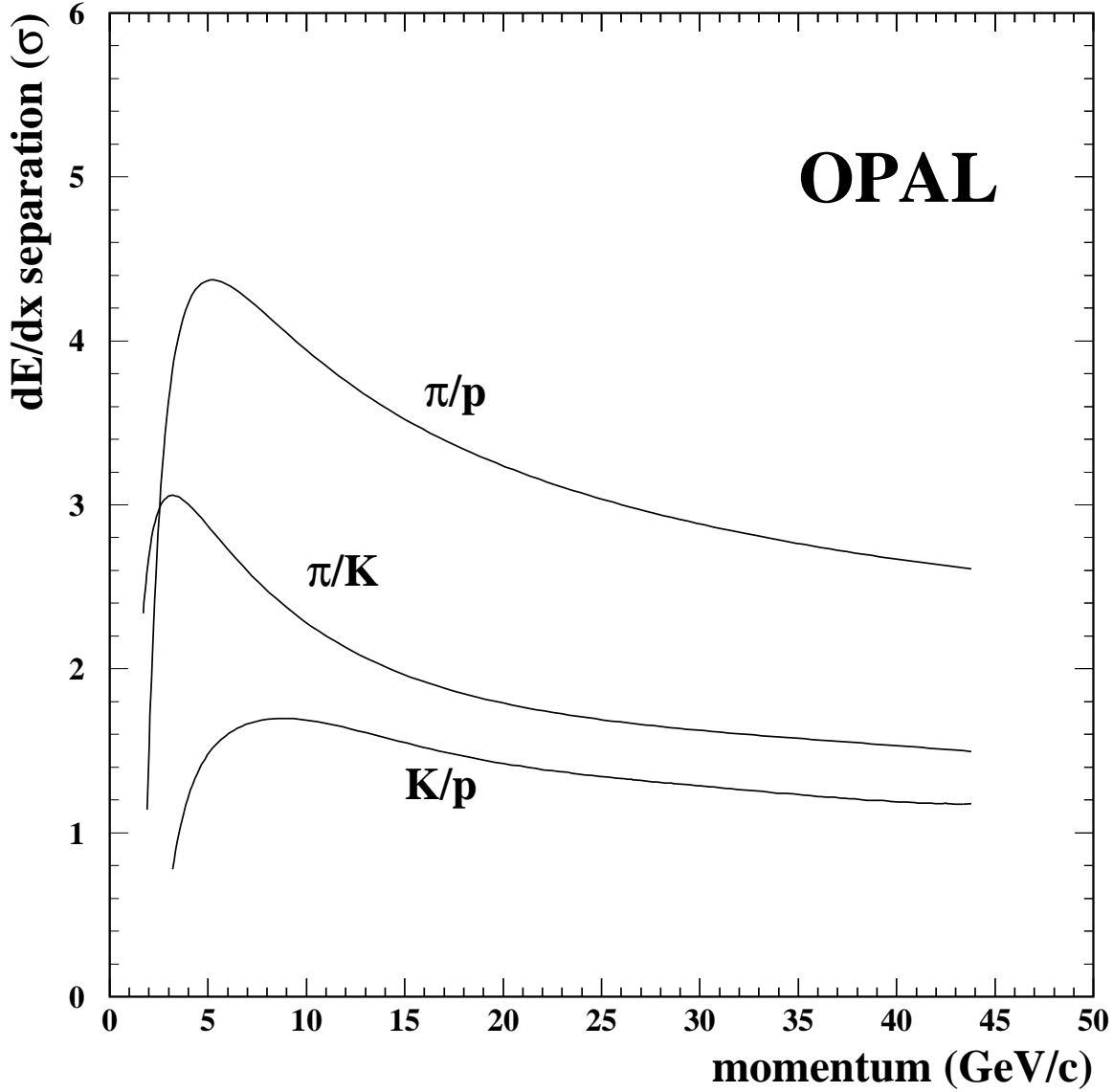


Figure 1: Two particle separation power $(dE/dx_1 - dE/dx_2)/\langle\sigma(dE/dx)\rangle$ in units of mean dE/dx resolution as a function of particle momentum for tracks with $|\cos\theta| < 0.7$ and at least 20 measured samples, obtained from data. The curves given are for pion/proton, pion/kaon and kaon/proton separation.

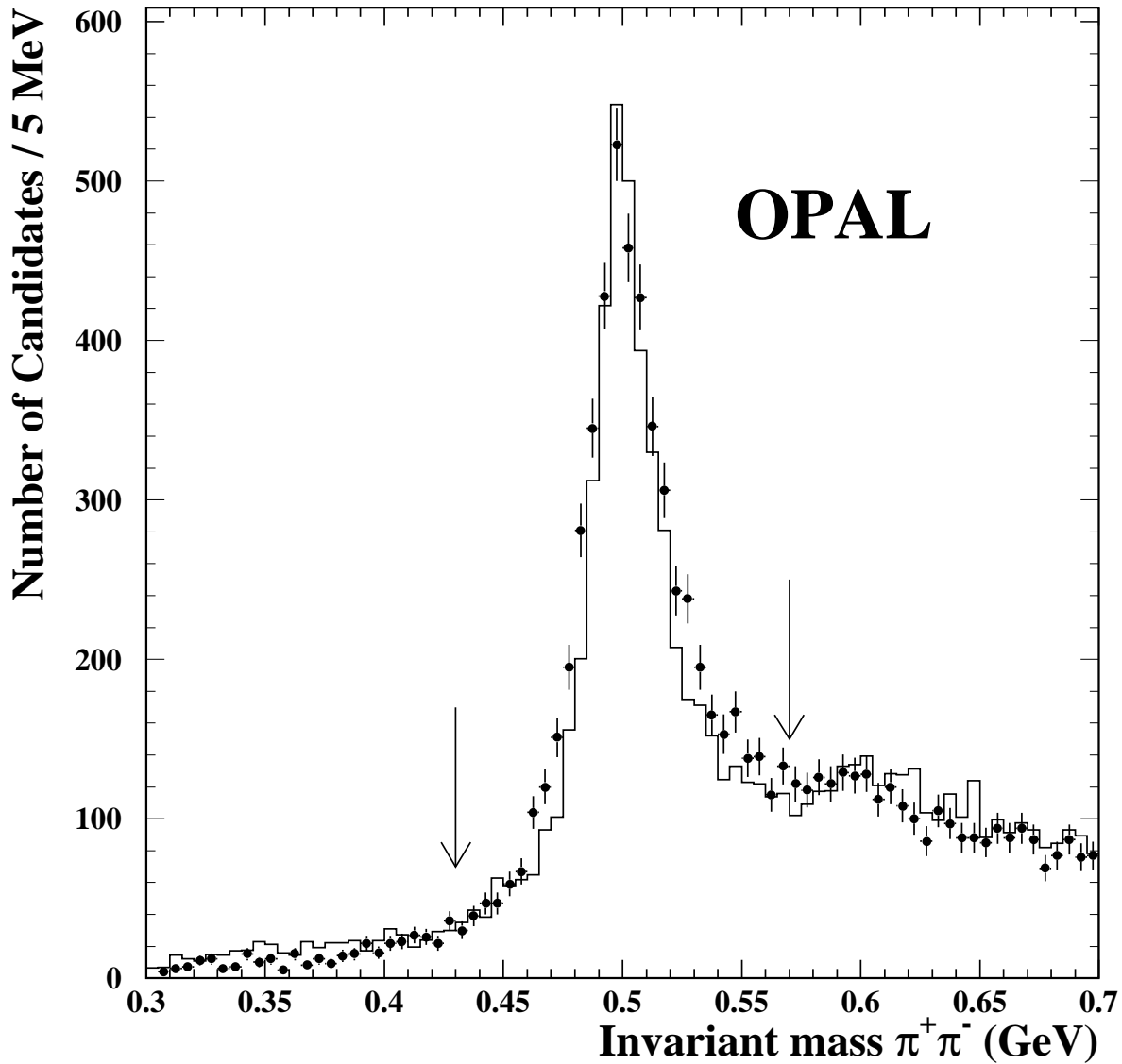


Figure 2: Invariant mass $\pi^+\pi^-$ of K_S^0 candidates with $x_p > 0.5$ in the data (points with error bars) compared to Monte Carlo (histogram) which is normalised to the same number of Z^0 events. Note that the details of the total K_S^0 production rate in the Monte Carlo are not relevant to this analysis. The arrows indicate the mass range in which K_S^0 candidates are selected as high- x_p tags. The different mass resolutions in the data and Monte Carlo are taken into account in the efficiency determination.

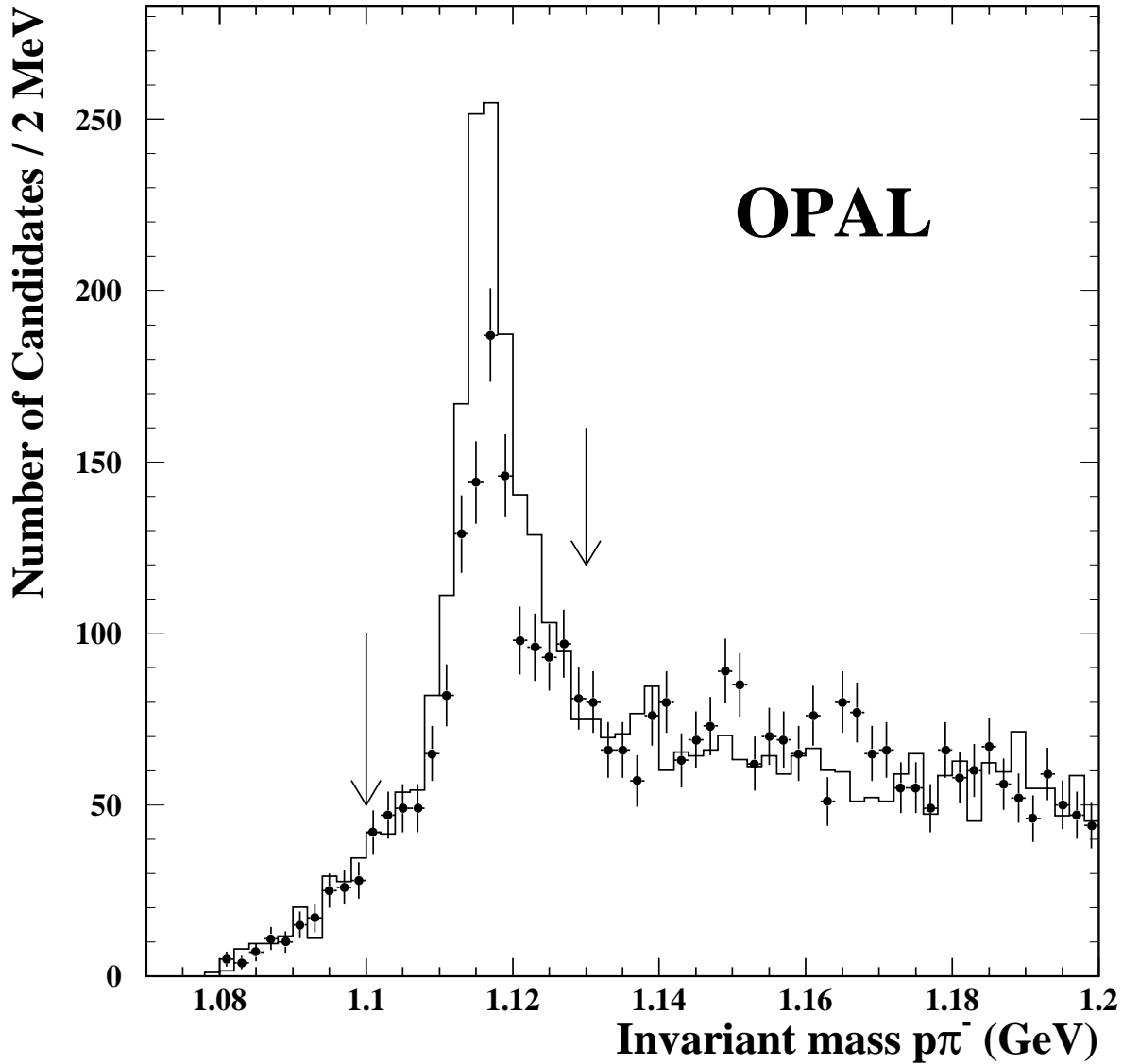


Figure 3: Invariant mass $p\pi^-$ of Λ candidates with $x_p > 0.5$ in the data (points with error bars) compared to Monte Carlo (histogram) which has been normalised to the same number of Z^0 events. The arrows indicate the mass range in which Λ candidates are selected as high- x_p tags. Note that the Λ fragmentation function is too hard in JETSET, resulting in an overestimation of the high- x_p production of Λ baryons, and that the details of the total Λ production rate in the Monte Carlo are not relevant to this analysis.

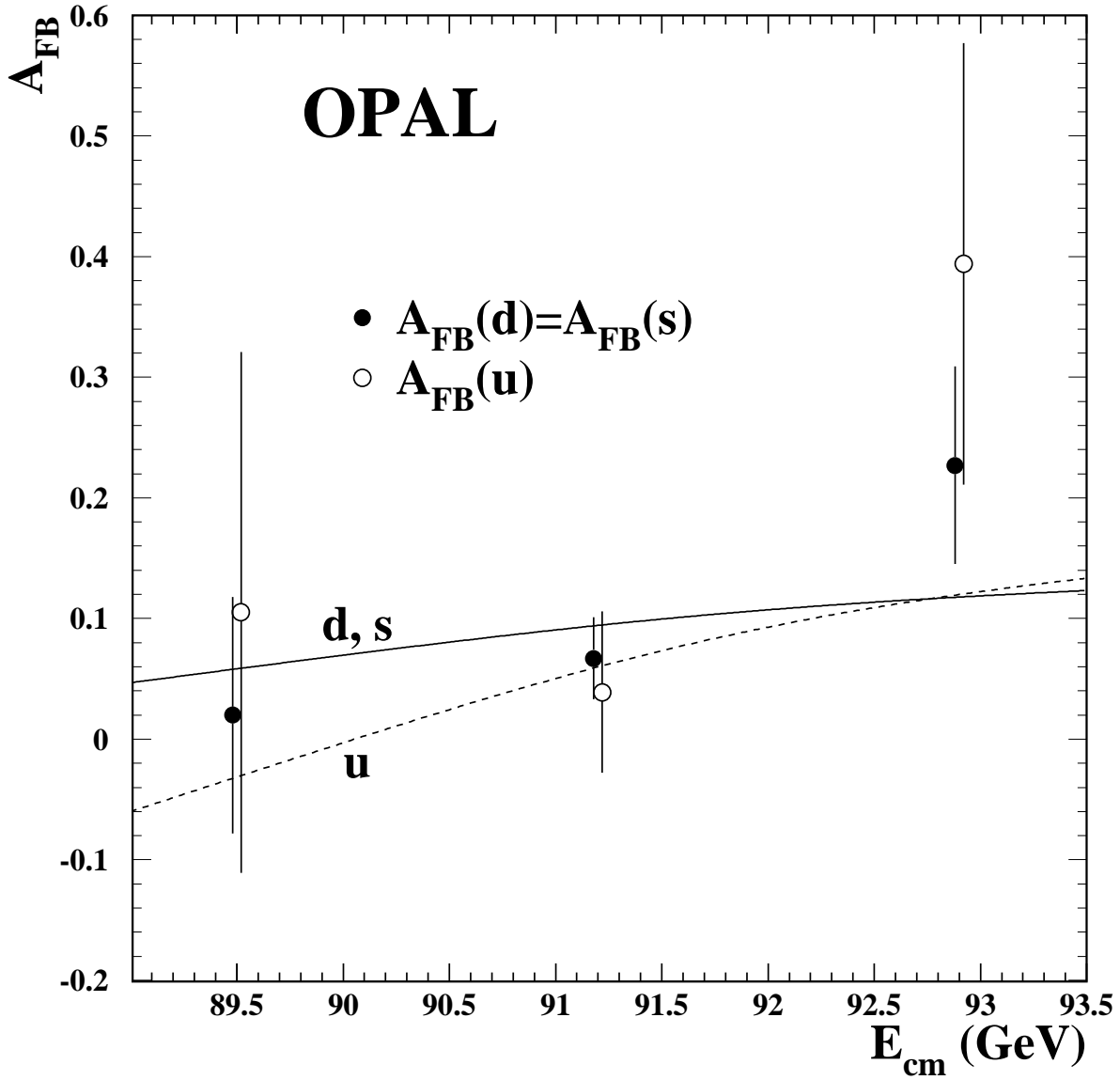


Figure 4: $A_{FB}(d,s)$ and $A_{FB}(u)$ versus the centre-of-mass energy, E_{cm} , where the errors are statistical plus systematic. The statistical errors for different centre-of-mass energies are uncorrelated. The systematic errors are correlated between centre-of-mass points. The Standard Model predictions for $m_{top} = 175$ GeV and $m_{Higgs} = 300$ GeV are shown as the solid curve for $A_{FB}(d,s)$ and the dashed curve for $A_{FB}(u)$.

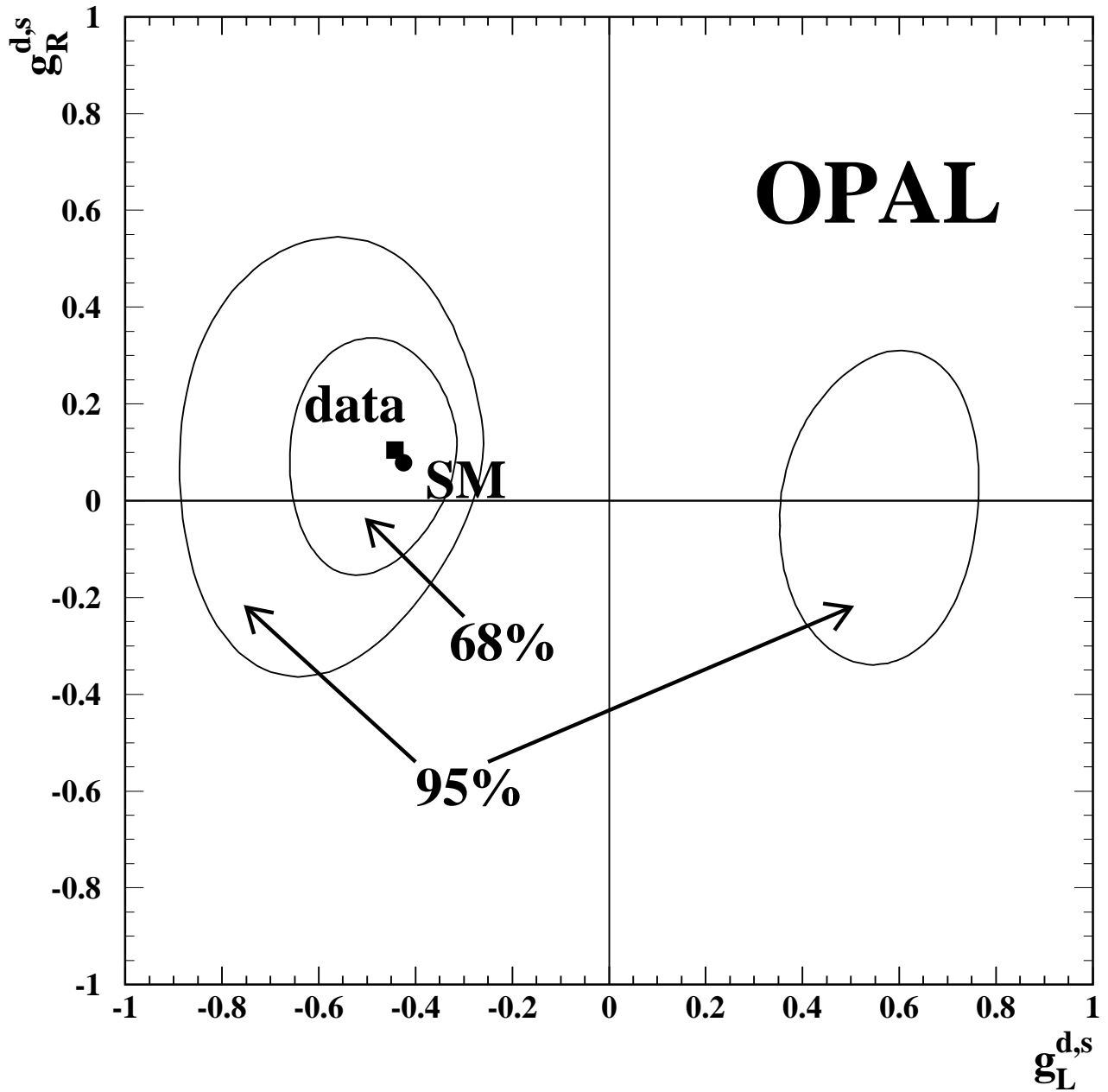


Figure 5: Left vs. right handed couplings of strange quarks, assuming identical values for down quarks. The 68% and 95% confidence level regions are also shown. The points correspond to the measurement and the Standard Model expectation.

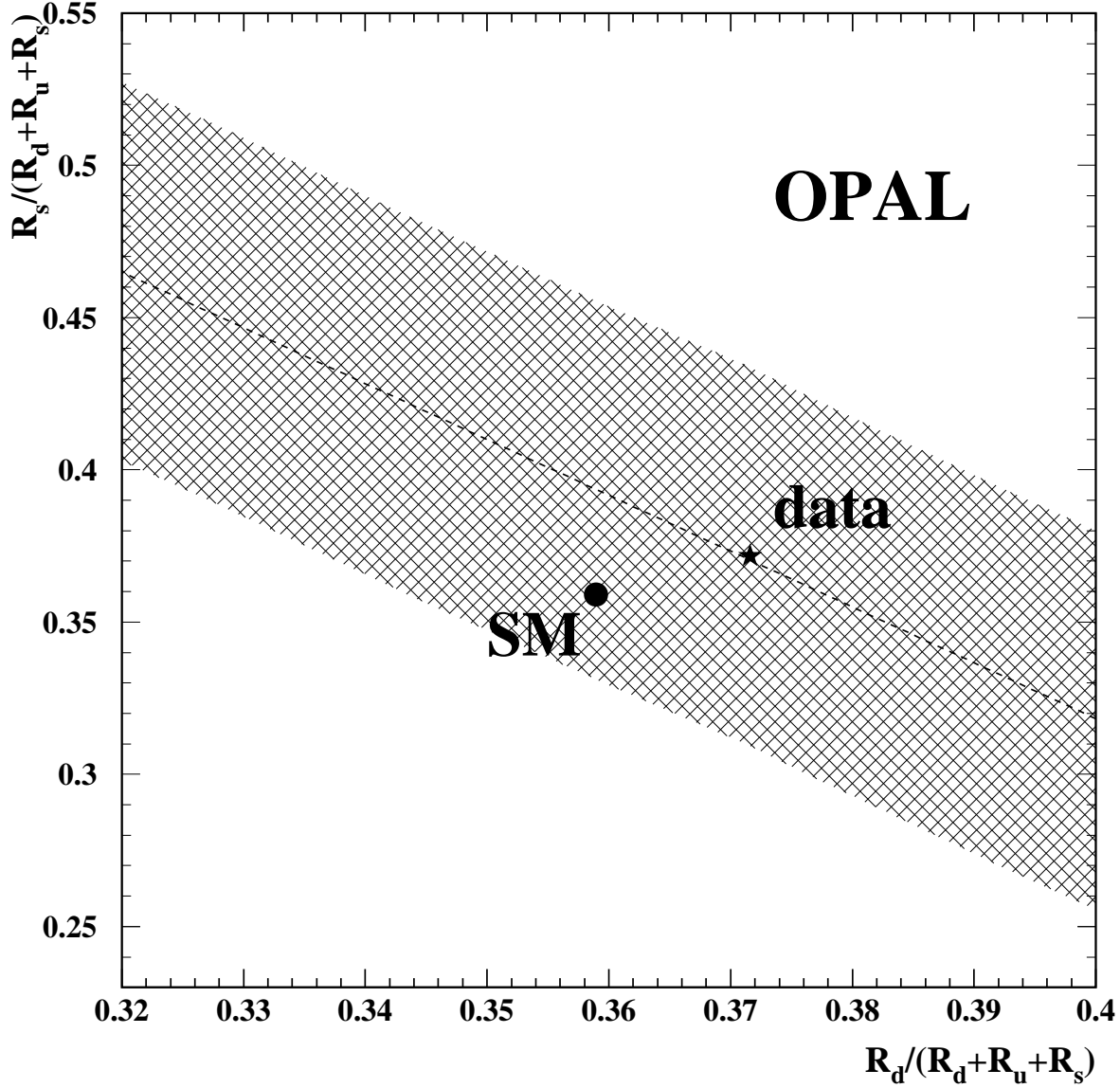


Figure 6: $R'_s = R_s/(R_d+R_u+R_s)$ determined for various fixed values of $R'_d = R_d/(R_d+R_u+R_s)$. The result obtained by enforcing the equality of R'_d and R'_s is given as the star, and the Standard Model value is shown as the solid point. The hatched region shows the total error on R'_s for a given R'_d . Note that $R'_u = 1 - R'_d - R'_s$.

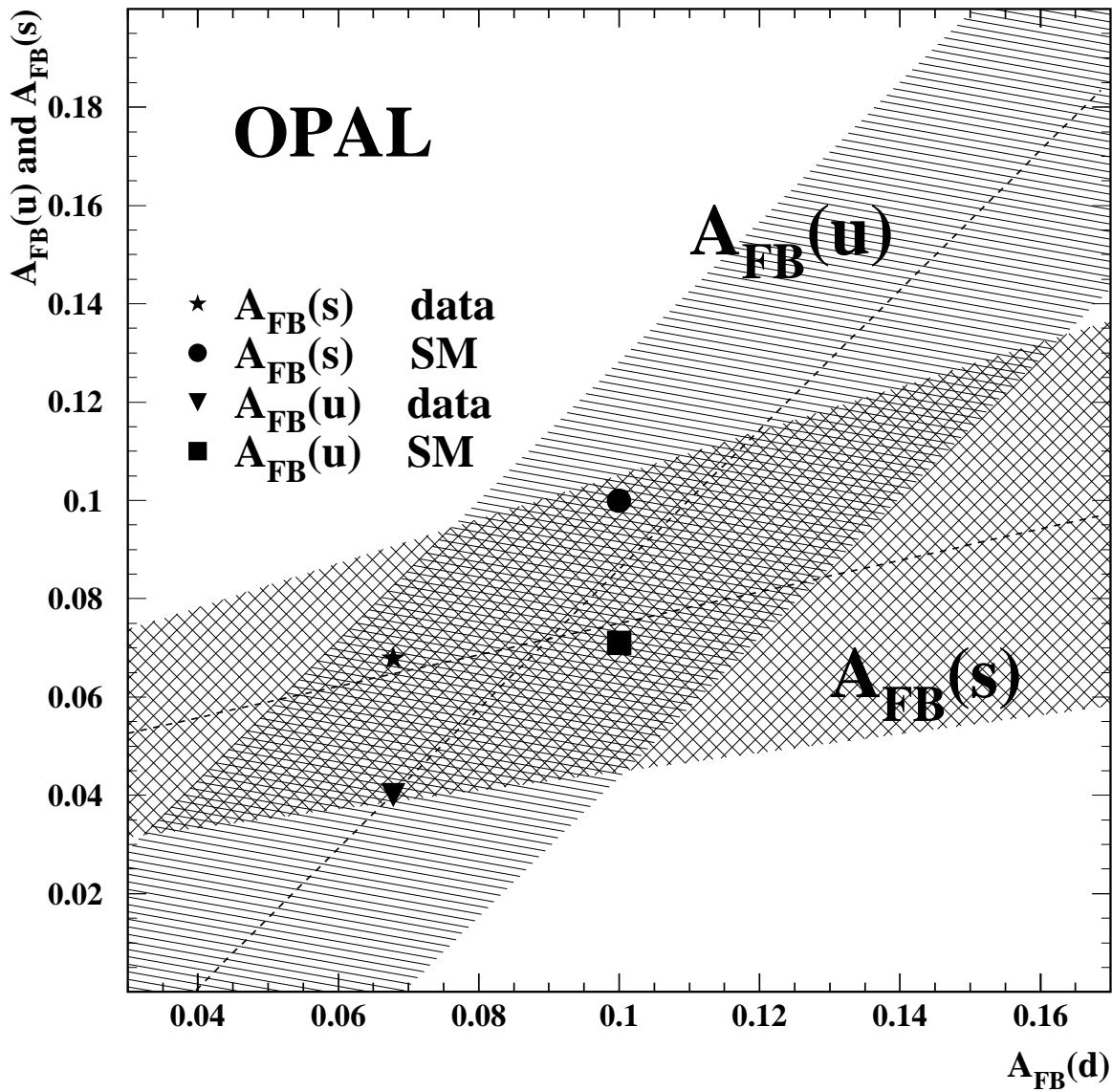


Figure 7: $A_{FB}(s)$ and $A_{FB}(u)$ determined for various fixed values of $A_{FB}(d)$. The results obtained by enforcing the equality of the down-type light flavour couplings are shown as the triangle and the star and the Standard Model values are shown as the square and circle for u and s quarks, respectively. The single and double hatched regions show the total error on $A_{FB}(u)$ and $A_{FB}(s)$, respectively, for a given $A_{FB}(d)$.